Collection of Boundary Conditions for One- and Some Multi-Dimensional Unsteady Flows of Polytropic Gases

J.J. Gottlieb * C.P.T. Groth **

ABSTRACT

The prescription of boundary data to obtain numerical solutions of the hyperbolic partial differential equations governing one- and some multi-dimensional unsteady flows of thermally and calorically perfect (polytropic) gases within confined stream tubes such as ducts and pipes is studied in a comprehensive and unified manner as Dirichlet-type boundary conditions for the following: (a) reflecting surfaces such as stationary solid walls, moving pistons and closed ends of ducts or pipes; (b) non-reflecting or transmissive boundaries; (c) subsonic and supersonic inflow and outflow boundaries using prescribed flow conditions; and (d) flux-tube boundaries or duct ends having inflow or outflow to and from both finite- and infinite-volume reservoirs. The unsteady flow conditions at these boundaries are all formulated on the basis of conventional and extended Riemann problems, and the solutions of these initial-value problems are presented as algebraic expressions for the dependent primitive variables (i.e., pressure, density, sound speed and flow velocity) at the boundaries in terms of the local interior solution and boundary imposed constraints. Several numerical examples are used to demonstrate the applicability of these Dirichlet boundary solutions in computations of one- and two-dimensional flow fields.

Key words: boundary conditions, Riemann problem, initial value problem, Euler equations, random-choice method.

RÉSUMÉ

La prescription des données de borne pour obtenir les solutions numériques des équations differentielles partielles hyperboliques régissant les écoulements instables uni- ou multi- dimensionnels des gaz thermiquement et caloriquement parfaits (polytropiques) dans des tubes de jet confinés, tels que des tuyaux et des pipes, est étudiée de façon approfondie et unifiée, en tant que conditions de

suite à la page 162

*Institute for Aerospace Studies
University of Toronto, 4925 Dufferin Street, North York
Ontario, Canada, M3H 5T6, E-mail: gottlieb@bach.utias.utoronto.ca
**Space Physics Research Laboratory
Department of Atmospheric, Oceanic and Space Sciences
University of Michigan, Ann Arbor
Michigan 48109-2143, USA
After 1 July 1999: * (UTIAS)

NOMENCLATURE

Alphanumeric Symbols

a	sound speed (m/s)
a_p	piston acceleration (m/s^2)
A	duct cross-sectional area (m^2)
c_p	specific heat at constant pressure (J/kg•K)
c_v	specific heat at constant volume (J/kg•K)
h	specific internal enthalpy (J/kg)
m_p	piston mass (kg)
M	flow Mach number (u/a)
M_s	shock Mach number relative to the flow in front
p	pressure (Pa)
Q	Mach number defined as $\lambda u/a$ or $\lambda\{u - v_p\}/a$
R	gas constant (J/kg•K)
S	set of state properties, i.e., S(p, a, u, γ, R)
t	time (s)
T	temperature (K)
u, v	flow velocities (m/s) in the x and y directions
v_p	piston velocity (m/s)
V_s	shock velocity (m/s)
x, y	Cartesian coordinate distances (m)
x_p	piston location (m)

Greek Symbols

γ	ratio of specific heats (c_p/c_v)
δ	orifice half-width (m)
ϵ	specific internal energy (J/kg)
λ	non-dimensional duct end parameter; $\lambda = -1$ for a left-side boundary and $\lambda = +1$ for a right-side boundary
ρ	density (kg/m^3)

Subscripts

1, 2	spatial locations in flow in a duct
e	node at edge of grid
i, n	node location and time value
o	reservoir, atmospheric, stagnation or prescribed state
*	undefined value

INTRODUCTION

The application of boundary conditions in the field of gas dynamics has a long history dating back to the earliest analytical and numerical methods for solving ordinary and partial differential equations. Some of the most relevant history for the case of hyperbolic partial differential equations that govern

suite de la page 161

borne de type-Dirichlet pour les suivants: (a) surfaces reflétantes telles que les murs solides stationnaires, les pistons mobiles et les extrémités fermées des tuyaux ou des pipes; (b) les bornes non- reflétantes ou transmissives; (c) les bornes d'apport et de sortie subsoniques et supersoniques, en utilisant des états prescrits d'écoulement; et (d) les bornes de flux-tube ou les extrémités de tuyau se rapportant en apport ou en sortie à des réservoirs au volume fini ou infini. Toutes les conditions d'écoulement instables à ces bornes sont formulées à base des problèmes conventionnels et approfondis de Riemann, et les solutions de ces problèmes de valeur initiale sont présentées en tant qu'expressions algébriques pour les variables primitives dépendantes (c.-à-d., pression, densité, vitesse sonique et vitesse d'écoulement) aux bornes en termes de la solution intérieure locale et des contraintes imposées par la borne. Plusieurs exemples numériques sont employés pour démontrer l'application des solutions de borne de Dirichlet dans les calculs des domaines d'écoulement uni-et bi- dimensionnels.

Mots clés: État de borne, problème de Riemann, problème de valeur initiale, équations d'Euler, méthode de choix aléatoire.

one-dimensional unsteady flows of polytropic gases is available in Rudinger's book (1955(a)). For example, he discusses boundary conditions and provides algebraic solutions for the cases of a closed duct end, a moving piston, and a duct end that is open to the atmosphere. Some of Rudinger's papers (1955(b,c,d), 1957, 1958, 1961(a,b,c)) also contain these and additional contributions, especially for the cases of a duct end that is open directly to the atmosphere and indirectly via a constricting plate with an orifice. Other early work of significance consists of studies of one-dimensional unsteady wave motion in shock tubes and in the pipes of reciprocating pumps and combustion engines by Bannister and Mucklow (1948), Mucklow and Wilson (1955), Benson (1959) and Ali, Gill and Imrie (1978), in which the boundary conditions for unsteady flow at a closed duct end and a duct end open to the atmosphere are considered as an integral part of their analyses and subsequent calculations.

In more recent studies, Clarke (1984(a,b,c)) investigated the reflection of weak shock waves from the closed end of a duct for which the reflecting surface was porous, absorbent and perforated, whereas Zhang and Gottlieb (1986) reconsidered more complete boundary conditions for the duct end open to the atmosphere. Although the analysis of this latter work is more comprehensive and standardized as compared to earlier work, it is nonetheless restricted to the case for which the duct and atmospheric gases are identical.

Artificial non-reflecting or transmissive boundary conditions that are appropriate for use with higher-order finite-difference solution procedures have also received considerable attention. Engquist and Majda (1977) have developed non-reflecting boundary conditions for linear hyperbolic systems in several space dimensions, and Hedstrom (1979) has proposed similar conditions for the non-linear case in one space dimension with an emphasis on the one-dimensional equations of gas dynamics. Further discussion of artificial boundary conditions for one-dimensional hyperbolic systems is given by Karni (1991), and Thompson (1987) has extended the concepts of Hedstrom (1979) to develop non-reflecting boundary conditions for the multi-dimensional case in terms of non-orthogonal coordinate systems. Additional theoretical and numerical work on non-reflecting boundary conditions for the Euler equations has been presented by Giles (1990).

From a mathematical and numerical viewpoint it is important to ensure that boundary conditions for initial boundary-value problems of one-dimensional gas flows are well posed and stable. An initial boundary-value problem is deemed to be well posed if a unique solution not only exists but is also bounded in the sense that small perturbations in boundary data give rise to small changes in the solution. Because most hyperbolic systems, such as the one-dimensional equations of gas dynamics, stem from the modelling of physical phenomena, their initial-value problems should necessarily be well posed.

Furthermore, when constructing numerical solutions to initial boundary-value problems, the combination of the interior solution procedure and boundary scheme ought to be stable. Kreiss (1970) and Higdon (1986) each discuss the well posedness of initial boundary-value problems for hyperbolic systems, and the question of stability has been studied for linear problems by Gustafsson, Kreiss and Sundström (1972). In addition, the stability of various choices of supersonic outflow boundary conditions for both linear and non-linear one-dimensional hyperbolic equations has been investigated by Kamowitz (1988).

The purpose of this paper is to provide a comprehensive and unified presentation of boundary conditions commonly required in the numerical simulation of one-dimensional unsteady flows of thermally and calorically perfect (polytropic) gases. A collection of Dirichlet boundary conditions and solutions are described for the cases of a closed duct end, moving piston, non-reflecting or transmissive pipe end, duct end with prescribed flow conditions, and duct end that is open either to a finite-volume reservoir or to an infinitely large atmosphere. These boundary conditions are all formulated in the same consistent manner on the basis of conventional and extended Riemann problems. This formulation differs somewhat conceptually from previous approaches that are based on the

at the boundary nodes are obtained on the basis of the known solution state at the adjacent interior node as well as additional information or analysis specific to the boundary type. For example, the solution for boundary state S_{i+4}^{n+1} requires that state S_{i+3}^{n+1} be known and additional information or analysis must be supplied specific to the type of boundary under consideration. This additional analysis, the type of wave pattern that occurs next to the boundary node, and the resulting algebraic boundary solution are the subject of this paper.

The solutions for the boundary conditions that will be presented are, strictly speaking, formulated only for the homogeneous form of Equation 1 (i.e., for $\mathbf{H} = 0$). However, experience has demonstrated that these boundary solutions may also be applied in the more general case for which the inhomogeneous terms are nonzero, because these terms can be integrated into the computational solution using an operator-splitting approach (see Sod, 1977; Groth and Gottlieb, 1988). Within the context of the preceding formulation the boundary solutions are necessarily explicit and first-order accurate.[b] The boundary solutions to be described are therefore ideally suited for solving one-dimensional unsteady flows using explicit first-order numerical schemes that are constructed on the basis of the Riemann problem, such as the random-choice method (Glimm, 1965; Chorin, 1976; Sod, 1977, Colella, 1982; Gottlieb, 1988) and Godunov's finite-volume method (Godunov, 1959). However, with special considerations it is possible to incorporate the present solutions for various boundaries into other, possibly higher-order, solution techniques.

In formulating boundary conditions in terms of the solutions to conventional and extended Riemann problems, extensive use is made of certain expressions that are fundamental solutions of Equation 1 for the case of shock waves, rarefaction waves, contact surfaces, and steady flows with area changes. Although these expressions already exist in books on gas dynamics, such as those by Zucrow and Hoffman (1976,1977), some relevant equations are summarized here for completeness so that they can be used in many different forms later in this paper.

Consider first the case of a shock wave that is either moving in a constant area duct or stationary in an oncoming steady supersonic flow (with or without an area change). The algebraic solution of Equation 1 with $\mathbf{H} = 0$ for the jump conditions across this thin entropic discontinuity (with a negligible area change), and for the shock velocity, can be expressed as

$$u_2 = u_1 \pm a_1 \frac{\frac{p_2}{p_1} - 1}{\gamma\sqrt{\frac{\gamma+1}{2\gamma}\frac{p_2}{p_1} + \frac{\gamma-1}{2\gamma}}}, \tag{3}$$

$$a_2 = a_1 \sqrt{\frac{(\gamma-1)(p_2/p_1)+(\gamma+1)}{(\gamma-1)(p_1/p_2)+(\gamma+1)}}, \tag{4}$$

$$\rho_2 = \rho_1 \frac{(\gamma+1)(p_2/p_1)+(\gamma-1)}{(\gamma-1)(p_1/p_2)+(\gamma+1)}, \tag{5}$$

$$V_s = u_1 \pm a_1 \sqrt{\frac{\gamma+1}{2\gamma}\frac{p_2}{p_1} + \frac{\gamma-1}{2\gamma}}, \tag{6}$$

with $\gamma = \gamma_1 = \gamma_2$ and $R = R_1 = R_2$. The subscripts 1 and 2 denote flow properties in front of and behind the shock wave, $p_2 \geq p_1$ for a shock wave to exist, V_s denotes the velocity of the shock wave in the laboratory frame of reference, and the positive and negative signs in Equations 3 and 6 are associated with shock waves propagating to the right and left, respectively. When $p_2 \to p_1$ the shock wave degenerates to a so-called Mach wave or Mach line across which there are vanishingly small changes in the flow properties. A shock Mach number $M_s = (V_s - u_1)/a_1$ can be defined for convenience with the frame of reference attached to the flow in front of the shock; then M_s is positive for rightward-propagating shock waves, negative for leftward-propagating shock waves, and $M_s^2 \geq 1$. If the flow properties of the initial state $S(p_1, a_1, u_1, \gamma_1, R_1)$ are known, then the final flow properties for state $S(p_2, a_2, u_2, \gamma_2, R_2)$ can be obtained if either p_2, a_2, ρ_2, u_2, V_s or M_s is specified.

Consider second the case of the rarefaction or expansion wave. The solution of Equation 1 with $\mathbf{H} = 0$ can be obtained by employing the theory or method of characteristics. The resulting algebraic expressions for the unsteady isentropic flow associated with a moving rarefaction wave in a constant-area duct can be expressed as

$$\frac{2}{\gamma-1}a_2 \pm u_2 = \frac{2}{\gamma-1}a_1 \pm u_1, \tag{7}$$

$$p_2 = p_1\left(\frac{a_2}{a_1}\right)^{\frac{2\gamma}{\gamma-1}} = p_1\left(\frac{\rho_2}{\rho_1}\right)^{\gamma}, \tag{8}$$

with $\gamma = \gamma_1 = \gamma_2$ and $R = R_1 = R_2$. The subscripts 1 and 2 denote the flow properties in front of and behind the rarefaction wave, $0 \leq p_2 \leq p_1$ for an expansion wave to exist, and the positive and negative signs in Equation 7 are associated with characteristic lines that cross rarefaction waves propagating to the left and right, respectively. When $p_2 \to p_1$ the expansion wave degenerates to a so-called Mach wave or Mach line (with vanishingly small changes in flow properties across a wave of vanishing strength, that is $p_2/p_1 - 1 \to 0$). If the initial state $S(p_1, a_1, u_1, \gamma_1, R_1)$ is known, then the final state $S(p_2, a_2, u_2, \gamma_2, R_2)$ can be determined if either p_2, a_2, ρ_2 or u_2 is specified.

Consider third the case of a moving contact surface, which is either the surface of contact between two different unmixed gases or the surface that separates two parts of the same gas that have different sound speeds and densities. The solution of Equation 1 with $\mathbf{H} = 0$ for this trivial case can be expressed as $p_2 = p_1$ and $u_2 = u_1$, in which the subscripts 1 and 2 denote the flow properties on the two sides of the contact surface. In other

[b]The order of accuracy is due primarily to the use of solution information only from the nearest interior node, rather than also making use of solution gradient information.

words, the contact surface is convected by the gas at its flow velocity while the gas pressure remains the same on each side of the surface, but flow and gas properties other than the pressure and flow velocity change discontinuously across this surface. This surface becomes indistinguishable when all changes in flow and gas properties become vanishingly small.

Consider the last case of a steady isentropic flow in a duct with an area change. The solution of Equation 1 with **H** consisting of

$$-\rho u \frac{1}{A}\frac{dA}{dx},$$

$$-\rho u^2 \frac{1}{A}\frac{dA}{dx}$$

and

$$-\rho u\left(\epsilon + \frac{1}{2}u^2 + \frac{p}{\rho}\right)\frac{1}{A}\frac{dA}{dx}$$

for the duct area variation with distance can also be obtained for such steady flows as

$$a_2^2 + \frac{\gamma-1}{2}u_2^2 = a_1^2 + \frac{\gamma-1}{2}u_1^2 = a_o^2, \qquad (9)$$

$$p_2\left(\frac{a_o}{a_2}\right)^{\frac{2\gamma}{\gamma-1}} = p_2\left(\frac{\rho_o}{\rho_2}\right)^{\gamma} = p_1\left(\frac{a_o}{a_1}\right)^{\frac{2\gamma}{\gamma-1}} = p_1\left(\frac{\rho_o}{\rho_1}\right)^{\gamma} = p_o, \qquad (10)$$

$$\rho_2 A_2 u_2 = \rho_1 A_1 u_1 = \rho_o A_o u_o, \qquad (11)$$

with $\gamma = \gamma_1 = \gamma_2 = \gamma_o$ and $R = R_1 = R_2 = R_o$. The subscripts 1 and 2 denote flow conditions corresponding to spatial locations 1 and 2 at which the finite duct areas are A_1 and A_2, respectively, the subscript o denotes reservoir or stagnation conditions (for which $u_o \to 0$ and $A_o \to \infty$), and the last equation represents the conservation of mass at two different duct locations. If the initial state $S(p_1, a_1, u_1, \gamma_1, R_1)$ is known, then the final state $S(p_2, a_2, u_2, \gamma_2, R_2)$ can be determined if either p_2, a_2, ρ_2 or u_2 is specified.

The Riemann problem is a special initial-value problem that can be expressed as

$$S(x,t^n) = \begin{cases} S(x_i, t^n) & \text{if } x_i < x < \frac{1}{2}(x_i + x_{i+1}), \\ S(x_{i+1}, t^n) & \text{if } \frac{1}{2}(x_i + x_{i+1}) \le x < x_{i+1}, \end{cases} \qquad (12)$$

where $S(x_i, t^n)$ is an initially known state $S_{left} \equiv S(p_{left}, a_{left}, u_{left}, \gamma_{left}, R_{left})$ at node (x_i, t^n) and $S(x_{i+1}, t^n)$ is an initially known right state $S_{right} \equiv S(p_{right}, a_{right}, u_{right}, \gamma_{right}, R_{right})$ at node (x_{i+1}, t^n). Hence, the initial cell data $S(x, t^n)$ is piecewise constant; it equals either S_{left} in the left half or S_{right} in the right half of the cell. At times larger than t^n this discontinuity breaks into leftward- and rightward-facing shock and rarefaction waves that are separated by a contact surface, as illustrated by the wave patterns in **Figure 2**. These five patterns are all self-similar (i.e., depend on x/t only), and the pattern type and the shock- and rarefaction-wave strengths depend on the initial conditions given by S_{left} and S_{right}. The solution of the Riemann problem to determine the pattern type and two intermediate states S^*_{left} and S^*_{right} between the contact surface and the leftward- and rightward-facing waves is based on the previous equations for shock and rarefaction waves and contact surfaces. Although the solution procedure is iterative, the solution can be obtained easily. For all physically realistic values of the state variables p, a, u, γ and R in both initial states S_{left} and S_{right}, the solutions for the pattern type and intermediate states S^*_{left} and S^*_{right} not only exist but also are unique. See Gottlieb and Groth (1988) for more details on the Riemann problem and its solution.

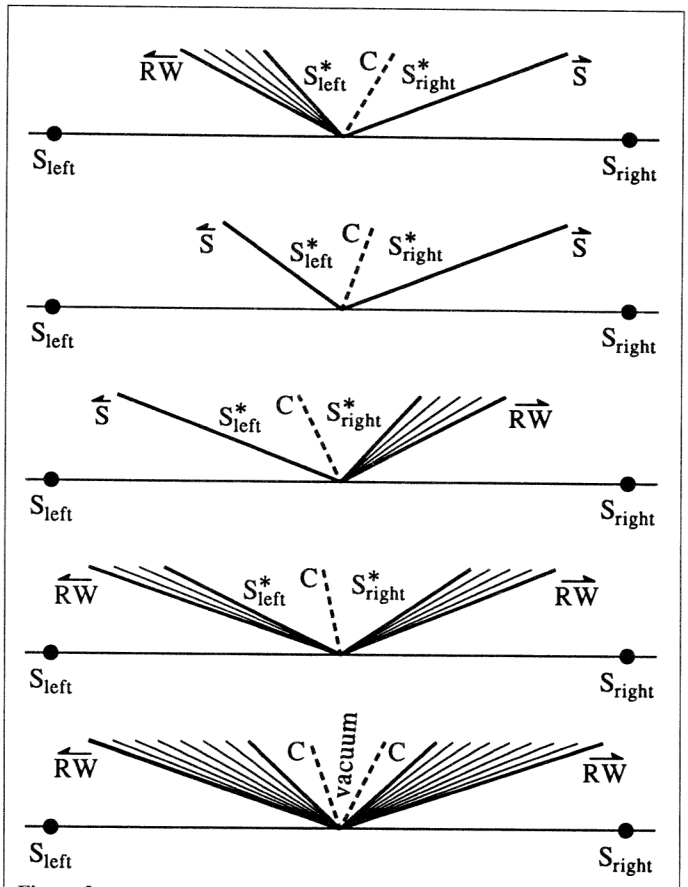

Figure 2.
Five possible wave patterns for the conventional Riemann problem for different left and right states S_{left} and S_{right}.

Reflecting Boundary Conditions

Numerical grids that contain or end at a moving or stationary solid boundary in the form of a moving piston or closed duct end are common in numerical computations. The application of boundary conditions for unsteady flows near or at such surfaces is treated in this section on the basis of the conventional Riemann problem (Gottlieb and Groth, 1988) described in the previous section. Based on this method, three distinct solutions

of the Riemann problem (or parts thereof) containing different types of wave motion or wave patterns can be formulated to patch the flow to the piston motion or closed duct end, with each wave pattern depending on the boundary velocity and local flow conditions adjacent to the moving or stationary boundary. These wave patterns are shown in **Figure 3** for the case of the right end of a grid adjacent to a moving solid boundary. The equivalent wave patterns corresponding to the converse case of the left end of the grid are mirror images of those shown in **Figure 3**.

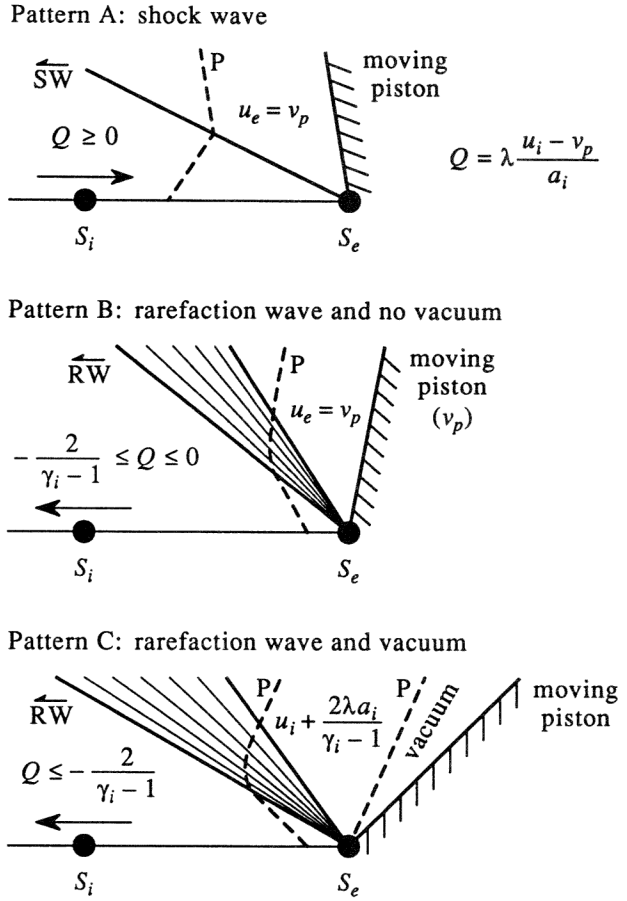

Figure 3.
Three possible wave patterns for unsteady flow at the right end of a grid for a moving solid piston ($v_p \neq 0$) and closed duct end ($v_p = 0$).

For wave pattern A in **Figure 3** the flow velocity at the interior node is larger than the boundary velocity and a leftward-propagating shock wave (SW) is thereby required such that this wave suddenly changes the velocity of the flow to that (v_p) of the solid boundary, as illustrated by the path (P) of the fluid particle. For wave pattern B the velocity of the flow is smaller than that of the boundary and a leftward-propagating rarefaction wave (RW) is required to smoothly alter the velocity of the flow to that of the boundary. In the case of wave pattern C the flow velocity at the interior node is so much smaller than the boundary velocity that the strongest possible leftward-propagating rarefaction wave is unable to completely change the velocity of the flow to that of the moving boundary. The resulting velocity mismatch between the piston velocity v_p and the flow velocity $u_i + 2\lambda a_i/(\gamma_i - 1)$ behind the rarefaction wave produces a growing vacuum region adjacent to the piston or boundary. Note that the flow velocity at the interior node and the boundary velocity are denoted in **Figure 3** by u_i and v_p, respectively, $Q = \lambda(u_i - u_p)/a_i$ with $\lambda = +1$ for the right-side boundary shown in **Figure 3**, γ_i is the specific-heat ratio at the interior node, and $v_p = 0$ for the particular case of a stationary piston or closed duct end. Additionally, $S(p_e, a_e, u_e, \gamma_e, R_e)$ is the solution state for the boundary node, and $S(p_i, a_i, u_i, \gamma_i, R_i)$ denotes the known state at the interior node next to the boundary node.

To solve the Riemann problem for the boundary conditions and determine the state $S(p_e, a_e, u_e, \gamma_e, R_e)$ for the case of wave pattern A with the shock wave (**Figure 3**), Equations 3 - 5 can be used almost directly. With the nearest interior state $S(p_i, a_i, u_i, \gamma_i, R_i)$ known and the boundary velocity $u_e = v_p$ specified, a rearrangement of Equation 3 yields the pressure p_e, and Equations 4 and 5 then yield a_e and ρ_e. The final results for this boundary state are

$$p_e = p_i \left[1 + \frac{1}{4}\gamma_i(\gamma_i + 1)Q^2 + \gamma_i Q \sqrt{1 + \frac{1}{16}(\gamma_i+1)^2 Q^2} \right],$$

$$a_e = a_i \sqrt{\frac{(\gamma_i-1)(p_e/p_i)+(\gamma_i+1)}{(\gamma_i-1)(p_i/p_e)+(\gamma_i+1)}}, \qquad (13)$$

$$\rho_e = \rho_i \frac{(\gamma_i+1)(p_e/p_i)+(\gamma_i-1)}{(\gamma_i-1)(p_e/p_i)+(\gamma_i+1)},$$

$$u_e = v_p, \ \gamma_e = \gamma_i, \ R_e = R_i,$$

in which $Q = \lambda(u_i - v_p)/a_i$ is a relative Mach number. The parameter λ is incorporated in the definition of Q such that this boundary solution is valid for pattern A at either end of the grid; $\lambda = +1$ for the right grid end with the shock-wave pattern shown in **Figure 3**, whereas $\lambda = -1$ for the left grid end with the mirror image of this pattern. For the reflecting boundary solution to contain the leftward-propagating shock, $Q \geq 0$ must be satisfied.

In the second case of wave pattern B with the rarefaction wave and no vacuum region, the solution of the Riemann problem to determine state $S(p_e, a_e, u_e, \gamma_e, R_e)$ is governed by Equations 7 and 8 and the specified condition that $u_e = v_p$. The resulting expressions that define the boundary state are

$$p_e = p_i \left[1 + \frac{\gamma_i - 1}{2} Q \right]^{\frac{2\gamma_i}{\gamma_i - 1}},$$

$$a_e = a_i \left[1 + \frac{\gamma_i - 1}{2} Q \right], \qquad (14)$$

$$\rho_e = \rho_i \left[1 + \frac{\gamma_i - 1}{2} Q\right]^{\frac{2}{\gamma_i - 1}},$$

$$u_e = v_p,\ \gamma_e = \gamma_i,\ R_e = R_i,$$

in which the relative Mach number $Q = \lambda(u_i - v_p)/a_i$ again includes the parameter λ so that the boundary solution is generalized to include both the left and right boundaries of the discretized flow field. For the reflecting boundary solution to contain the leftward-propagating rarefaction wave and no vacuum region, $-2/(\gamma_i - 1) \leq Q \leq 0$ must occur.

For the last case of wave pattern C with the rarefaction wave and vacuum region the solution of the Riemann problem for the boundary state $S(p_e, a_e, u_e, \gamma_e, R_e)$ can be given as

$$p_e = 0,\ a_e = 0,\ \rho_e = 0,\ u_e = u_*,\ \gamma_e = \gamma_*,\ R_e = R_*, \qquad (15)$$

for the case of either end of a grid with a moving boundary, in which u_*, γ_* and R_* denote values that are undefined because this state occurs at a node in the vacuum region. For the reflecting boundary solution to contain the leftward-propagating rarefaction wave and vacuum region, $Q \leq -2/(\gamma_i - 1)$ must hold. Note that this case of a wave pattern with an ideal vacuum state is possible theoretically,[c] although it does not have much practical application and should rarely if ever be encountered when solving gasdynamic problems in engineering. Of more importance at low pressures and temperatures is the departure from perfect-gas behaviour owing to the real-gas effects of molecular vibration and liquefaction.

The boundaries and domains for the three possible wave patterns corresponding to the moving piston and closed-end boundary are presented in **Figure 4** as a map of the pressure p_i versus the relative Mach number Q. The two boundaries that separate the three patterns, given by $Q_{AB} = 0$ and $Q_{BC} = -2/(\gamma_i - 1)$, and details of the Riemann boundary solution demonstrate that the three wave-pattern domains cover the theoretically meaningful pressure and Mach-number ranges

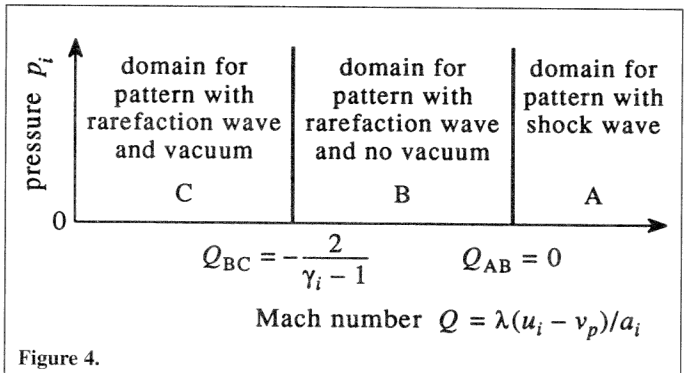

Figure 4.
Boundaries and domains of the three possible wave patterns for a moving solid piston ($v_p \neq 0$) and closed duct end ($v_p = 0$).

[c]A piston could be pulled faster than a gas could follow. If a vacuum state occurred during numerical computations, then special considerations would be required in the code to track the spatial extent of the vacuum region, such that flow computations inside the vacuum region could be over-stepped.

defined by $0 \leq p < \infty$ and $-\infty < Q < +\infty$ without any gaps or overlaps. Hence, the preceding three algebraic solutions for state $S(p_e, a_e, u_e, \gamma_e, R_e)$ for moving and stationary solid boundaries are comprehensive and give unique solution states for all realistic values of the state $S(p_i, a_i, u_i, \gamma_i, R_i)$ and boundary velocity v_p.

If the preceding reflecting boundary conditions are implemented in conjunction with the random-choice and similar methods (Chorin, 1976; Sod, 1977; Colella, 1982; Gottlieb, 1988), then it is possible that a layer of gas next to a solid boundary and having given values of γ and R can become compressed from an initial width of many cells into a single cell next to the boundary. This layer of gas may subsequently be lost from the numerical flow field due to the assignment of different values of γ and R associated with the next gas layer that was originally farther away from the boundary. This should not be interpreted as a failure of the solution procedure or boundary conditions. The loss of the original gas near the boundary should instead be attributed to the use of a grid that is too coarse to adequately resolve the basic flow-field features. Grid refinement will reduce this error.

Computations that advance the flow-field solution in time can be supplemented to also advance the solution for the piston or projectile motion. The basic equations for tracking the piston motion are given here. The applications of boundary conditions at the piston back and front surfaces S_b and S_f determine these boundary states at time level t^n. The application of Newton's second law of motion then yields an equation for the piston acceleration a_p, and subsequent integrations give the velocity v_p and displacement x_p. The results are

$$a_p = \alpha + \beta \Delta t,$$

$$v_p = v_p^n + \alpha \Delta t + \frac{1}{2}\beta \Delta t^2, \qquad (16)$$

$$x_p = x_p^n + v_p^n \Delta t + \frac{1}{2}\alpha \Delta t^2 + \frac{1}{6}\beta \Delta t^3,$$

in which the piston motion is considered from time t^n to a larger time t (e.g., t^{n+1}), and $\alpha = (p_b^n - p_f^n)(A/m_p)$, $\beta = \alpha[(\gamma\, p/a)_b^n + (\gamma\, p/a)_f^n](A/m_p) = \alpha[(\rho a)_b^n + (\rho a)_f^n](A/m_p)$, A is the duct cross-sectional area, m_p denotes the piston mass, $\Delta t = t - t^n$, and the superscript n indicates state values at the n^{th} time level. The last term in each of these equations stems from the higher-order effects of a non-constant piston velocity produced by changes in the piston back and front pressures p_b and p_f as time increases in one time level. More specifically, the production of additional weak shock and expansion waves at the front and rear of an accelerating projectile, beyond those already occurring in the conventional Riemann problem, are included here as a linearized correction. These higher-order terms improve the accuracy of the predicted piston path. Note that additional forcing terms other than those already included in Equation 16, such as the force arising from friction between the piston and duct-wall surfaces, can be incorporated in these equations when they are required.

Non-Reflecting Boundary Conditions

The numerical grid used in many computations of one-dimensional unsteady gas flows is often truncated artificially at the left and/or right ends of the solution domain before the real flow field and duct actually end, and non-reflecting or transmissive boundary conditions are commonly used at these locations. This flow field truncation is done primarily to reduce the size of the computational domain and thereby reduce the computational effort required to obtain a numerical solution. Such a flow field truncation is normally done judiciously such that the most important features of the actual flow field are contained within the grid and undesirable influences of the artificial boundaries are usually inconsequential.

In the case of a non-reflecting or transmissive end of a duct, shock waves, rarefaction waves and contact surfaces that are moving towards the grid edge must be transmitted across the grid boundary without the undesirable occurrence of a reflected wave in the computational domain. Four Riemann problems (or parts thereof) can be formulated such that no wave of finite amplitude is reflected from or produced by the boundary, and each of these problems depends on local subsonic and supersonic flow conditions adjacent to the boundary. These four wave patterns are illustrated in **Figure 5** for the case of subsonic and supersonic inflows and outflows. The equivalent patterns for the opposite case of the left grid end are mirror images of those shown in **Figure 5**.

Wave pattern A in **Figure 5** for the case of supersonic inflow has leftward-propagating and rightward-propagating Mach waves (MW) separated by a leftward-moving contact surface (C_0). Changes in the gas and flow properties across these Mach waves and the contact surface are negligible, and the rightward-propagating but leftward-swept Mach wave exists in pattern A because it is swept leftward by the faster moving oncoming supersonic inflow and cannot leave the grid. Wave pattern B for the case of subsonic inflow contains only a leftward-propagating Mach wave and leftward-moving contact surface; a rightward-propagating Mach wave would leave the grid because it moves faster than the oncoming subsonic inflow. Pattern C for the case of subsonic outflow has only a leftward-propagating Mach wave, because a contact surface would be convected off the grid by the subsonic outflow. In the last case of pattern D there are no waves because the supersonic outflow sweeps the slower moving leftward-facing Mach wave off the grid.

The Mach waves and contact surfaces in the wave patterns in **Figure 5** should have negligible changes in flow and gas properties across them in order to satisfy the boundary constraint that no reflected wave or contact surface of finite amplitude should arise at the non-reflecting boundary. The solutions of the Riemann problems for all four wave patterns are trivial and obtained simply by setting the state $S(p_e, a_e, u_e, \gamma_e, R_e)$ at the boundary equal to the state $S(p_i, a_i, u_i, \gamma_i, R_i)$ at the adjacent interior node; hence,

$$p_e = p_i,\ a_e = a_i,\ \rho_e = \rho_i,\ u_e = u_i,\ \gamma_e = \gamma_i,\ R_e = R_i \qquad (17)$$

is the desired solution for either end of the numerical grid with a non-reflecting boundary. This non-reflecting boundary solution is essentially a constant-extrapolation boundary condition (Kamowitz, 1988).

The boundaries and domains for the four possible wave patterns associated with the non-reflecting boundary are illustrated as a map of the pressure versus Mach number in **Figure 6**. The Mach number is formulated as $Q = \lambda u_i/a_i$ to include boundaries on both the right ($\lambda = +1$) and left ($\lambda = -1$) sides of the grid. The three boundaries that separate the four patterns, given by $Q_{AB} = 1$, $Q_{BC} = 0$ and $Q_{CD} = -1$ demonstrate that the four wave-pattern domains cover the theoretically meaningful pressure and Mach-number ranges defined by $0 \le p < \infty$ and $-\infty < Q < +\infty$ without gaps or overlaps. Hence, the algebraic solutions for state $S(p_e, a_e, u_e, \gamma_e, R_e)$ for non-reflecting or transmissive boundaries are comprehensive and give unique solution states for all realistic values of the state $S(p_i, a_i, u_i, \gamma_i, R_i)$.

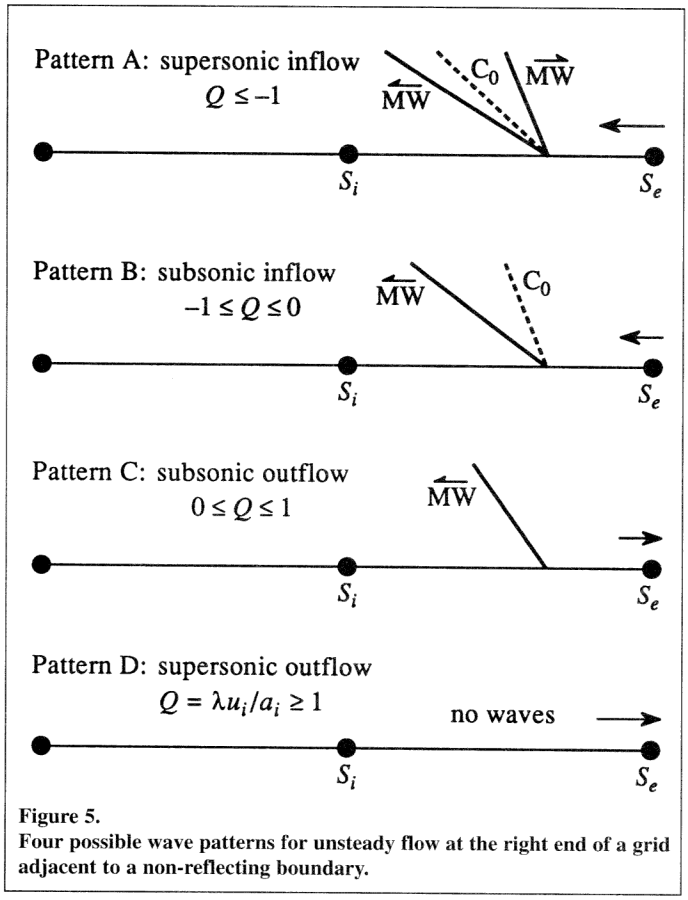

Figure 5.
Four possible wave patterns for unsteady flow at the right end of a grid adjacent to a non-reflecting boundary.

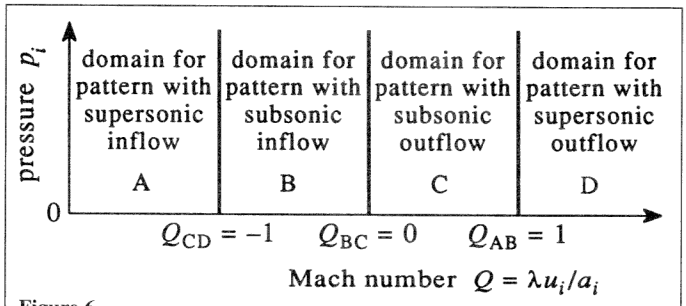

Figure 6.
Boundaries and domains of the four possible wave patterns for a non-reflecting boundary.

The non-reflecting boundary solutions should be used with caution because they are invariably artificial and only an approximation to actual unsteady boundary flow conditions. The degree of approximation is problem specific. For example, in the case of a supersonic outflow in which shock and expansion waves cannot travel upstream, this boundary solution becomes exact. For the cases of subsonic outflow and subsonic and supersonic inflows, these boundary solutions are invariably incorrect. In the latter case, the state of the inflowing gas at the boundary is dictated entirely by the interior solution that does not necessarily represent accurately the physical processes occurring outside the grid where the inflow originates. The non-reflecting boundary solution would obviously give incorrect results for cases in which the grid is truncated just before a flow obstruction like a closed end, a rapid area change or an open duct end, because each of these would otherwise produce a strong disturbance that would enter the computational domain.

In other cases the adverse effects of using non-reflecting boundary conditions in one-dimensional flowfield predictions are less subtle but can nonetheless be important. For example, unsteady flows in ducts with wall friction and heat transfer continually produce leftwardly and rightwardly running weak waves that can eventually produce significant changes in actual flow fields. In addition, a decaying shock wave (i.e., a shock being overtaken by a rarefaction wave) produces an entropy gradient and a reflected wave that can become significant. Furthermore, the interactions of shock and rarefaction waves with each other as well as with entropy gradients or contact regions can also produce additional reflected waves that can become important in modifying the actual flow field. The artificial truncation of a grid and the use of non-reflecting boundary solutions does not permit the prediction of reflected waves from processes that occur outside the computational domain. Hence, the possible influences of such reflected waves, if they should have entered the computational flow field, are neglected. See Hedstrom (1979) and Thompson (1987) for alternate discussions and several examples that further illustrate the limitations of non-reflecting boundary conditions.

Prescribed Boundary Conditions

Prescribed, pre-specified or imposed boundary conditions are frequently used at the end of a numerical grid that has been truncated artificially or otherwise, primarily to reduce the computational effort and determine a smaller than actual flow field. The objective of prescribing boundary conditions is to force the flow field to undergo temporal changes in order that it conform to or relax towards the prescribed boundary data at the grid edge, often in an iterative process of determining a steady-state flow field. To achieve this objective, let the prescribed state desired at the grid edge be denoted by $S(p_o, a_o, u_o, \gamma_o, R_o)$, independent of the boundary state solution $S(p_e, a_e, u_e, \gamma_e, R_e)$ at the grid edge, and note that $S(p_i, a_i, u_i, \gamma_i, R_i)$ is the state at the interior node next to the boundary node. The problem of prescribing boundary conditions is then reduced to a determination of the boundary state $S(p_e, a_e, u_e, \gamma_e, R_e)$ in terms of the prescribed state $S(p_o, a_o, u_o, \gamma_o, R_o)$ and interior state $S(p_i, a_i, u_i, \gamma_i, R_i)$. This determination is done on the basis of a boundary-flow analysis that includes a good physical model of the wave motion occurring at the boundary and some reasonable logic that makes or helps the flow field adjust or conform quickly to the prescribed boundary conditions.

Different methods of prescribing boundary conditions are possible because different sets of physical and logical arguments may be adopted. Some previous and new methods are presented in the following sections with comments such that the reader can decide which method is best for a particular application, because the implementation complexity and problem applicability can both vary significantly.

Imposed Boundary Solution

The boundary state $S(p_e, a_e, u_e, \gamma_e, R_e)$ in this imposed boundary-solution method is simply forced to equal the prescribed state $S(p_o, a_o, u_o, \gamma_o, R_o)$. The main advantages are that this method is simple and the desired solution for the boundary state is implemented fully and immediately. However, this simple method is not recommended because the main advantages can often be offset by the subsequent problem that the flow field computations might fail, or take a long time, to converge to the correct steady-state solution.

Characteristic theory can be used to show that such prescribed boundary data are over-determined for subsonic and supersonic inflows and subsonic outflows and determined correctly only for supersonic outflows; see Porter and Coakley (1972) for a discussion of characteristic boundary conditions. Some flow field computations illustrate that shock and rarefaction waves that approach the grid edge where the boundary data are unduly imposed tend to become trapped and dissipate very slowly, because realistic transmission and reflection processes are not permitted. Slow wave dissipation can increase markedly the computational effort for an initially unsteady flow field to conform to or relax towards the prescribed boundary conditions simultaneously as the flow field converges to the correct steady-flow solution. Nonetheless, this method is mentioned here because it can sometimes be used to produce meaningful numerical solutions of steady-state flow fields for some engineering problems that are not unduly sensitive to over-determined boundary data.

Boundary Solution Based on a Sampled Riemann Problem

The boundary state $S(p_e, a_e, u_e, \gamma_e, R_e)$ in this boundary-solution method based on a sampled Riemann problem is considered to occur midway between the interior grid node with state denoted by $S(p_i, a_i, u_i, \gamma_i, R_i)$ and a grid exterior 'ghost' node with the prescribed state $S(p_o, a_o, u_o, \gamma_o, R_o)$. A Riemann problem is constructed with the discontinuity at the grid edge midway between these nodes and uses the interior state $S(p_i, a_i, u_i, \gamma_i, R_i)$ and prescribed state $S(p_o, a_o, u_o, \gamma_o, R_o)$. This Riemann problem is solved to determine the intermediate state (Gottlieb and Groth, 1988), and thereby the types and strengths of these leftward and rightward propagating waves. The five possible wave patterns, depending on particular values associated with the interior and prescribed states, were shown earlier in **Figure 2**.

This Riemann solution is then sampled on the wave-pattern centreline and the resulting sampled state is assigned directly to the boundary state $S(p_e, a_e, u_e, \gamma_e, R_e)$.

The boundary solution S_e depends on the particular values of the states S_i and S_o. State S_e can consist entirely as state S_i for the case of a strong outflow for which the leftward propagating shock or rarefaction wave in the Riemann solution is swept off the grid, or entirely as state S_o for the opposite case of a strong inflow for which the rightward propagating shock or rarefaction wave in the Riemann solution is swept into the grid, or an intermediate state S^*_{left} or S^*_{right} (**Figure 2**) between the contact surface and leftward or rightward propagating waves, or some sampled state inside a leftward or rightward propagating rarefaction wave. Inflow or outflow at the grid edge can occur, depending on the particular states S_i and S_o. The boundary data for S_e are determined correctly in that they are not over- or under-determined, and waves encountering the grid edge are treated correctly in the analysis in that they are partially transmitted and reflected as dictated by states S_i and S_o.

The Riemann problem set-up and iterative solution is relatively simple and straightforward for computational methods that already are based on the Riemann problem to evalute fluxes into and out of cells, such as Godunov finite-volume method and the random-choice method. For other computational methods a suitably efficient Riemann solver would need to be programmed or borrowed.

The primary disadvantage of this boundary-solution strategy using a sampled Riemann problem is that the prescribed boundary state S_o may not exert as strong an influence as desirable on forcing the flow field to conform or adapt to the prescribed boundary state, because the boundary data assigned to state S_e result from a sampling of the Riemann problem between states S_i and S_o. This loose specification may be judged undesirable from the viewpoint that other boundary-solution methods can be devised to more strongly influence the flow field to conform to the prescribed state S_o.

Boundary Solution Based on a Riemann Problem

The boundary state $S(p_e, a_e, u_e, \gamma_e, R_e)$ in this boundary-solution method is formulated on the basis of the Riemann problem (or parts thereof) that uses both the prescribed state $S(p_o, a_o, u_o, \gamma_o, R_o)$ and interior state $S(p_i, a_i, u_i, \gamma_i, R_i)$. Boundary flows that are possible physically are selected in a logical manner such that the prescribed data have a strong influence on forcing the flow field to conform to the prescribed boundary state. The selection ensures that the boundary-solution data are not under- or over-determined, and that solutions are available for all possible values of the states S_i and S_o.

Our formulation results in six basic wave patterns shown in **Figure 7** for the right end of a grid. Wave pattern A has no waves because shock and rarefaction waves are unable to move upstream into the rightward-moving supersonic flow. Wave pattern B features a leftward-propagating shock wave (SW) that is sufficiently strong to move upstream and leaves a subsonic outflow, whereas in pattern C the leftward-propagating shock wave produces a subsonic or supersonic inflow that is apparent

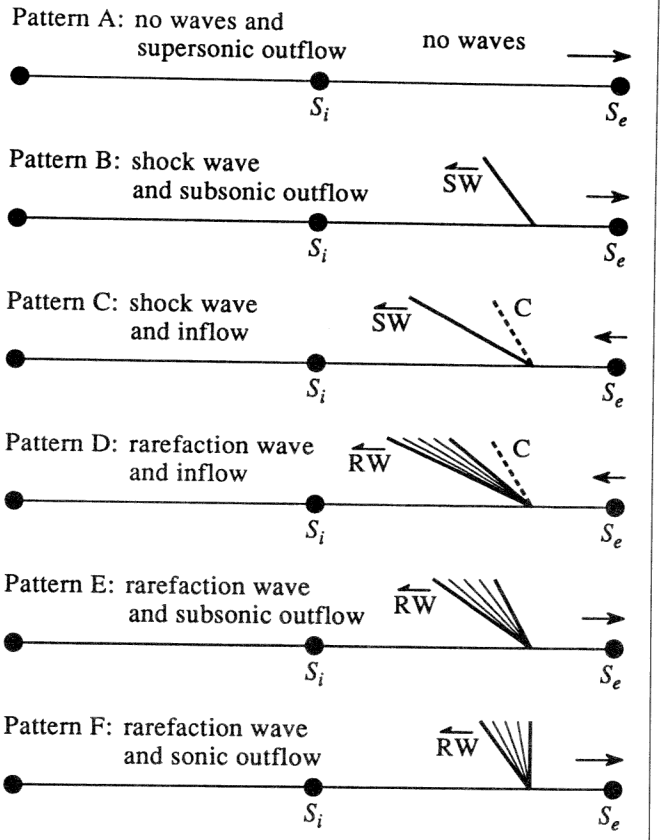

Figure 7.
Six basic wave patterns of shock and rarefaction waves for inflows and outflows at the right end of a grid at which boundary conditions are prescribed.

from the accompanying leftward-moving contact surface (C). Wave pattern D features a leftward-propagating rarefaction wave (RW) with a following contact surface and subsonic or supersonic inflow, whereas pattern E has a leftward-moving rarefaction wave with no trailing contact surface because of the subsonic outflow. Pattern F has a leftward-propagating rarefaction wave that accelerates the gas to a sonic outflow, as indicated by the vertical tail of the expansion wave. The corresponding wave patterns for the converse case of the left end of a grid are mirror images of those shown in **Figure 7**.

The boundaries and domains of wave patterns A to F are presented in **Figure 8** in the form of a map of the pressure ratio p_o/p_i versus the Mach number $Q = \lambda u_i/a_i$. The parameter Q is again formulated to include λ such that the diagram summarizes boundaries for both right ($\lambda = +1$) and left ($\lambda = -1$) grid ends. Domains C and D are subdivided into C_1 and C_2 and D_1 and D_2, respectively, to delineate between inflows that are subsonic (C_1, D_1) and supersonic (C_2, D_2). The ten boundaries that separate the eight wave patterns are described by the following algebraic equations:

$$Q_{AB} = \sqrt{\frac{\gamma_i+1}{2\gamma_i}\frac{p_o}{p_i} + \frac{\gamma_i-1}{2\gamma_i}} \quad \text{if } p_i \le p_o < \infty, \tag{18}$$

$$Q_{AF} = 1 \quad \text{if} \quad 0 \le p_o \le p_i, \tag{19}$$

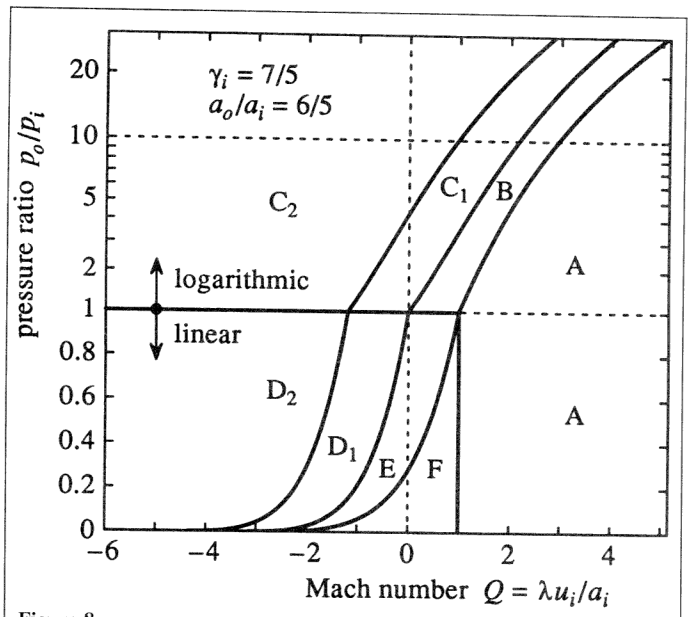

Figure 8.
Boundaries and domains of the six basic wave patterns for shock and rarefaction waves for prescribed boundary conditions.

$$Q_{BC_1} = \frac{\frac{p_o}{p_i} - 1}{\gamma_i \sqrt{\frac{\gamma_i + 1}{2\gamma_i} \frac{p_o}{p_i} + \frac{\gamma_i - 1}{2\gamma_i}}} \quad \text{if } p_i \le p_o < \infty, \tag{20}$$

$$0 \le Q_{BE} \le 1 \quad \text{if } p_o = p_i, \tag{21}$$

$$Q_{C_1C_2} = Q_{BC_1} - \frac{a_o}{a_i} \quad \text{if } p_i \le p_o < \infty, \tag{22}$$

$$-\frac{a_o}{a_i} \le Q_{C_1D_1} \le 0 \quad \text{if } p_o = p_i, \tag{23}$$

$$-\infty < Q_{C_2D_2} \le \frac{a_o}{a_i} \quad \text{if } p_o = p_i, \tag{24}$$

$$Q_{D_1D_2} = Q_{D_1E} - \frac{a_o}{a_i} \quad \text{if } 0 \le p_o \le p_i, \tag{25}$$

$$Q_{D_1E} = \frac{2}{\gamma_i - 1}\left(\frac{p_o}{p_i}\right)^{\frac{\gamma_i - 1}{2\gamma_i}} - \frac{2}{\gamma_i - 1} \quad \text{if } 0 \le p_o \le p_i, \tag{26}$$

$$Q_{EF} = \frac{\gamma_i + 1}{\gamma_i - 1}\left(\frac{p_o}{p_i}\right)^{\frac{\gamma_i - 1}{2\gamma_i}} - \frac{2}{\gamma_i - 1} \quad \text{if } 0 \le p_o \le p_i. \tag{27}$$

Some of these boundaries depend not only on the Mach number Q and pressure ratio p_o/p_i but also on the specific-heats ratio γ_i at the interior node and the sound speed ratio a_o/a_i. The results shown in **Figure 8** are for the particular case of $\gamma_i = 7/5$ (diatomic gas) and $a_o/a_i = 6/5$.

Boundary AB is the division between pattern A with a shock wave that is swept downstream and off the grid and pattern B with a shock wave that can propagate upstream on the grid, whereas boundary AF is the corresponding case for the head of the rarefaction wave. Hence, Equation 18 is obtained essentially by setting the shock-wave speed to zero (i.e., $V_s = 0$ in Equation 6), and Equation 19 is obtained directly from setting the speed of the rarefaction wave head to zero (i.e., $u_i - a_i = 0$). Boundaries BC_1 and D_1E mark the division between wave patterns with outflow and inflow; hence, Equations 20 and 26 are obtained essentially by setting the flow velocity equal to zero behind the shock wave (described by Equation 3) and the rarefaction wave (described by Equations 7 and 8), respectively. Boundaries C_1C_2 and D_1D_2 delineate subsonic and supersonic inflows. Boundary EF is the division between wave patterns in which the outflows behind a rarefaction wave are just subsonic and sonic; hence, Equation 27 is obtained from Equations 7 and 8 in conjunction with $u = a$ behind this expansion wave. The other boundaries BE, C_1D_1 and C_2D_2 given by Equations 21, 23 and 24 are obvious divisions between wave patterns that contain shock waves ($p_o/p_i \ge 1$) and rarefaction waves ($0 \le p_o/p_i \le 1$).

The solutions for the boundary data for all of these wave patterns with subsonic and supersonic inflows and outflows can be obtained algebraically and summarized as follows:

$$p_e = \begin{cases} p_i & \text{for pattern A,} \\ p_o & \text{for B, C, D and E,} \\ p_i\left(\dfrac{2}{\gamma_i + 1} + \dfrac{\gamma_i - 1}{\gamma_i + 1}\dfrac{\lambda u_i}{a_i}\right)^{\frac{2\gamma_i}{\gamma_i - 1}} & \text{for F,} \end{cases} \tag{28}$$

$$u_e = u_i - \begin{cases} 0 & \text{for pattern A,} \\ \dfrac{\lambda a_i\left(\dfrac{p_e}{p_i} - 1\right)}{\gamma\sqrt{\dfrac{\gamma_i + 1}{2\gamma_i}\dfrac{p_e}{p_i} + \dfrac{\gamma_i - 1}{2\gamma_i}}} & \text{for B and C,} \\ \dfrac{2\lambda a_i}{\gamma_i - 1}\left(\dfrac{p_e}{p_i}\right)^{\frac{\gamma_i - 1}{2\gamma_i}} - \dfrac{2\lambda a_i}{\gamma_i - 1} & \text{for D, E and F,} \end{cases} \tag{29}$$

$$a_e = \begin{cases} a_i & \text{for pattern A,} \\ a_i\sqrt{\dfrac{(\gamma_i - 1)(p_e/p_i) + (\gamma_i + 1)}{(\gamma_i - 1)(p_i/p_e) + (\gamma_i + 1)}} & \text{for B,} \\ a_o & \text{for C and D,} \\ a_i\left(\dfrac{p_e}{p_i}\right)^{\frac{\gamma_i - 1}{2\gamma_i}} = a_i + \lambda\dfrac{\gamma_i - 1}{2}(u_i - u_e) & \text{for E and F,} \end{cases} \tag{30}$$

$$\rho_e = \begin{cases} \rho_i & \text{for pattern A,} \\ \rho_i \dfrac{(\gamma_i + 1)(p_e/p_i) + (\gamma_i - 1)}{(\gamma_i - 1)(p_e/p_i) + (\gamma + 1)} & \text{for B,} \\ \rho_o & \text{for C and D,} \\ \rho_i \left(\dfrac{p_e}{p_i}\right)^{\frac{1}{\gamma_i}} & \text{for E and F,} \end{cases} \tag{31}$$

$$\gamma_e = \begin{cases} \gamma_i & \text{for patterns A, B, E and F} \\ \gamma_o & \text{for C and D,} \end{cases} \tag{32}$$

$$Re = \begin{cases} R_i & \text{for patterns A, B, E and F} \\ R_o & \text{for C and D.} \end{cases} \tag{33}$$

These solutions for the prescribed boundary data are not described in detail, but they are based partly on Equations 3 to 5 for shock waves in wave patterns B and C, partly on Equations 7 and 8 for rarefaction waves in wave patterns D, E and F, partly on previously given information that the pressure and flow velocity are the same on each side of the contact surface in wave patterns C and D, and partly on whether outflow or inflow occurs at the boundary.

The prescribed pressure p_o can be forced on the boundary node as p_e only for wave patterns B, C, D and E (see Equation 28). In the case of wave pattern A the boundary data $S(p_e, a_e, u_e, \gamma_e, R_e)$ is dictated entirely by $S(p_i, a_i, u_i, \gamma_i, R_i)$, because supersonic flow sweeps all waves off the grid. In the case of wave pattern F the lowest pressure that can be imposed at the boundary node is that which makes the outflow sonic (see the last expression in Equation 28). In all cases of outflow the solutions for γ_e and R_e are dictated by γ_i and R_i, because the gas flows from the interior node to the boundary node, whereas for the other case of inflows the solutions for a_e, ρ_e, γ_e and R_e can all be prescribed by a_o, ρ_o, γ_o and R_o. The boundary flow velocity u_e is always calculated, as can be seen from Equation 29, so it need not be prescribed. This situation occurs partly because only p_e or u_e can be prescribed across a single leftward propagating wave and the other must be calculated.

The solutions for the prescribed boundary data are comprehensive and unique because the boundaries and domains in **Figure 8** for the seven basic wave patterns for these prescribed boundary conditions cover the theoretically meaningful pressure and Mach-number ranges defined by $0 \leq p < \infty$ and $-\infty < Q < +\infty$ without gaps or overlaps, for all possible values of the states $S(p_i, a_i, u_i, \gamma_i, R_i)$ and $S(p_o, a_o, u_o, \gamma_o, R_o)$. This solution comprehensiveness and uniqueness is based mainly on the careful selection of matching flow or wave patterns for the grid boundary flows. A different selection of grid boundary flow patterns will result in a variation of the previous wave-pattern domains and boundary solutions. For example, for supersonic inflows the leftward propagating rarefaction wave with the leftward moving contact surface in pattern D might be changed to consist of a leftward moving contact surface with a rightward propagating rarefaction wave that is swept downstream onto the grid. Such simple changes can introduce wave-pattern domains with gaps or overlaps with resulting nonexistent or ambiguous solutions, respectively.

Boundary Solution Based on a Simplified Riemann Problem

Another fairly general approach is to formulate the boundary state $S(p_e, a_e, u_e, \gamma_e, R_e)$ on the basis of a simplified Riemann problem (or parts thereof) that uses both the prescribed state $S(p_o, a_o, u_o, \gamma_o, R_o)$ and interior state $S(p_i, a_i, u_i, \gamma_i, R_i)$ in a manner similar to that in the previous section. However, instead of using the conventional Riemann problem with shock and rarefaction waves separated by a contact surface, the shock waves are assumed weak and replaced by a compression wave. This approximation results in a simplification in the analysis of grid boundary flows, because the equations for compression and rarefaction waves are the same, and a distinction between these waves becomes unnecessary.

The formulation for the simplified Riemann problem for prescribed boundary conditions results in four basic wave patterns at the grid end, and these are shown in **Figure 9**. Wave pattern

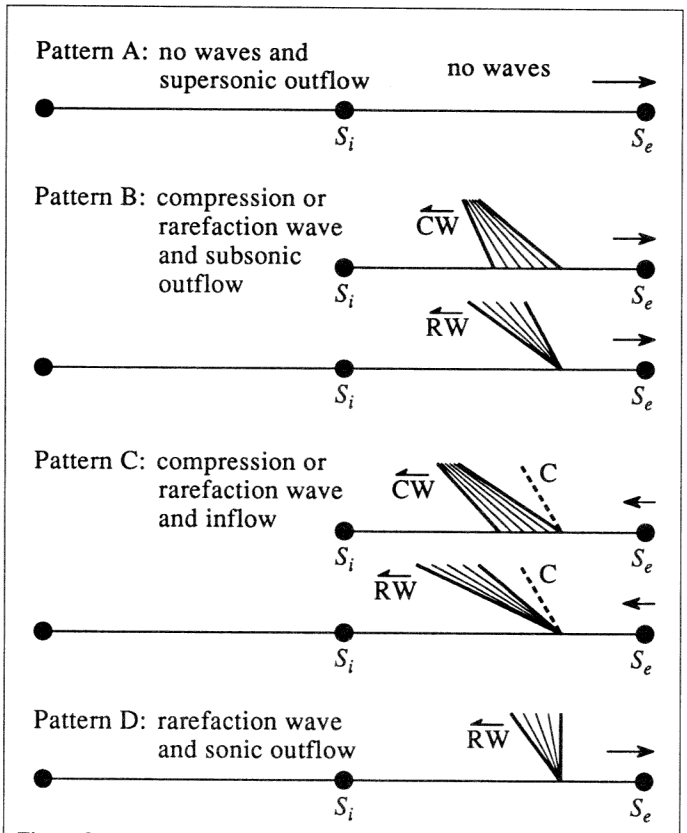

Figure 9.
Four basic wave patterns of compression and rarefaction waves for inflows and outflows at the right end of a grid at which boundary conditions are prescribed.

A has no waves because neither compression nor rarefaction waves can move upstream into the rightward-moving supersonic flow. Wave pattern B features a leftward-propagating compression wave (CW) or rarefaction wave (RW), and this isentropic wave moves upstream and leaves a subsonic outflow (no contact surface). In wave pattern C the leftward-propagating isentropic wave of compression or expansion produces a subsonic or supersonic inflow, which is evident by the leftward-moving contact surface (C). Wave pattern D features a leftward-propagating rarefaction wave that accelerates the gas to a sonic outflow. The equivalent wave patterns for the converse case of the left grid end are mirror images of those shown in **Figure 9**.

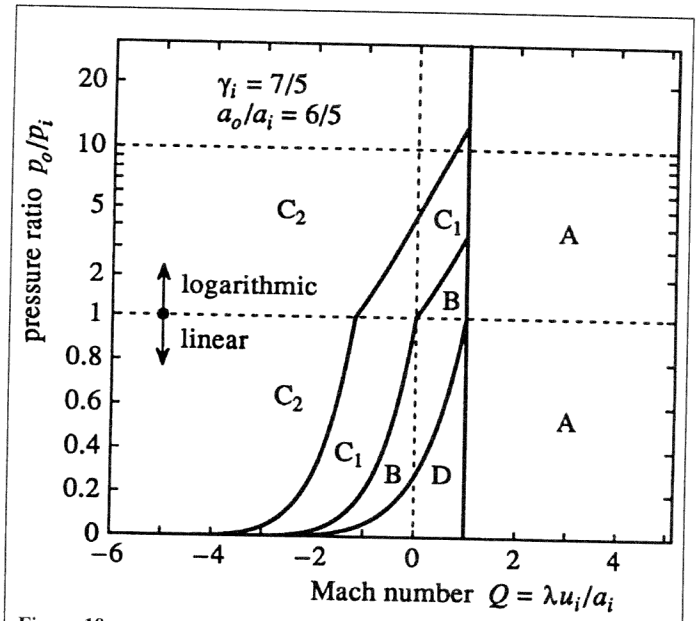

Figure 10.
Boundaries and domains of the four basic wave patterns of compression and rarefaction waves for prescribed boundary conditions.

The boundaries and domains of wave patterns A to D are shown in **Figure 10**, once again as a map of the pressure ratio p_o/p_i versus the Mach number Q = $\lambda u_i/a_i$. The parameter Q includes the parameter λ so that the diagram summarizes boundaries for both right ($\lambda = +1$) and left ($\lambda = -1$) grid ends. Domain C is further subdivided into C_1 and C_2 to delineate between inflows that are subsonic and supersonic, respectively. The seven boundaries that separate the five wave patterns are given by the following equations:

$$Q_{AB} = 1 \qquad \text{if } p_i \le p_o \le p_a, \tag{34}$$

$$Q_{AC_1} = 1 \qquad \text{if } p_a \le p_o \le p_b, \tag{35}$$

$$Q_{AC_2} = 1 \qquad \text{if } p_b \le p_o < \infty, \tag{36}$$

$$Q_{AD} = 1 \qquad \text{if } 0 \le p_o \le p_i, \tag{37}$$

$$Q_{BC_1} = \frac{2}{\gamma_i - 1}\left(\frac{p_o}{p_i}\right)^{\frac{\gamma_i - 1}{2\gamma_i}} - \frac{2}{\gamma_i - 1} \qquad \text{if } 0 \le p_o \le p_a, \tag{38}$$

$$Q_{C_1C_2} = Q_{BC_1} - \frac{a_o}{a_i} \qquad \text{if } 0 \le p_o \le p_b, \tag{39}$$

$$Q_{BD} = \frac{\gamma_i + 1}{\gamma_i - 1}\left(\frac{p_o}{p_i}\right)^{\frac{\gamma_i - 1}{2\gamma_i}} - \frac{2}{\gamma_i - 1} \qquad \text{if } 0 \le p_o \le p_i, \tag{40}$$

in which

$$p_a = p_i\left(\frac{\gamma_i + 1}{2}\right)^{\frac{2\gamma_i}{\gamma_i - 1}}$$

and

$$p_b = p_i\left(\frac{\gamma_i + 1}{2} + \frac{\gamma_i - 1}{2}\frac{a_o}{a_i}\right)^{\frac{2\gamma_i}{\gamma_i - 1}}.$$

Some of these boundaries depend not only on the Mach number Q and pressure ratio p_o/p_i but also the specific-heats ratio γ_i at the interior node and the sound speed ratio a_o/a_i, so the results in **Figure 10** are shown for the particular case of $\gamma_i = 7/5$ and $a_o/a_i = 6/5$.

The solutions for the boundary data for the wave patterns with subsonic and supersonic inflows and outflows can be obtained in algebraic form, and these solutions are summarized as follows:

$$p_e = \begin{cases} p_i & \text{for pattern A,} \\ p_o & \text{for B and C,} \\ p_i\left(\dfrac{2}{\gamma_i + 1} + \dfrac{\gamma_i - 1}{\gamma_i + 1}\dfrac{\lambda u_i}{a_i}\right)^{\frac{2\gamma_i}{\gamma_i - 1}} & \text{for D,} \end{cases} \tag{41}$$

$$u_e = u_i - \begin{cases} 0 & \text{for pattern A,} \\ \dfrac{2\lambda a_i}{\gamma_i - 1}\left(\dfrac{p_e}{p_i}\right)^{\frac{\gamma_i - 1}{2\gamma_i}} - \dfrac{2\lambda a_i}{\gamma_i - 1} & \text{for B, C and D,} \end{cases} \tag{42}$$

$$a_e = \begin{cases} a_i & \text{for pattern A,} \\ a_o & \text{for C,} \\ a_i\left(\dfrac{p_e}{p_i}\right)^{\frac{\gamma_i - 1}{2\gamma_i}} = a_i + \lambda\dfrac{\gamma_i - 1}{2}(u_i - u_e) & \text{for B and D,} \end{cases} \tag{43}$$

$$\rho_e = \begin{cases} \rho_i & \text{for pattern A,} \\ \rho_o & \text{for C,} \\ \rho_i\left(\dfrac{p_e}{p_i}\right)^{\frac{1}{\gamma_i}} & \text{for B and D,} \end{cases} \tag{44}$$

$$\gamma_e = \begin{cases} \gamma_i & \text{for patterns A, B and D} \\ \gamma_o & \text{for C,} \end{cases} \tag{45}$$

A has no waves because neither compression nor rarefaction waves can move upstream into the rightward-moving supersonic flow. Wave pattern B features a leftward-propagating compression wave (CW) or rarefaction wave (RW), and this isentropic wave moves upstream and leaves a subsonic outflow (no contact surface). In wave pattern C the leftward-propagating isentropic wave of compression or expansion produces a subsonic or supersonic inflow, which is evident by the leftward-moving contact surface (C). Wave pattern D features a leftward-propagating rarefaction wave that accelerates the gas to a sonic outflow. The equivalent wave patterns for the converse case of the left grid end are mirror images of those shown in **Figure 9**.

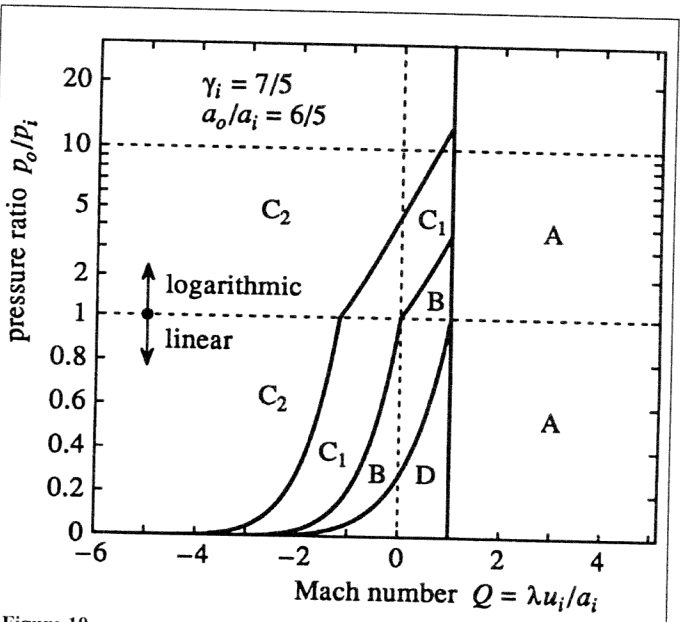

Figure 10.
Boundaries and domains of the four basic wave patterns of compression and rarefaction waves for prescribed boundary conditions.

The boundaries and domains of wave patterns A to D are shown in **Figure 10**, once again as a map of the pressure ratio p_o/p_i versus the Mach number Q = $\lambda u_i/a_i$. The parameter Q includes the parameter λ so that the diagram summarizes boundaries for both right ($\lambda = +1$) and left ($\lambda = -1$) grid ends. Domain C is further subdivided into C_1 and C_2 to delineate between inflows that are subsonic and supersonic, respectively. The seven boundaries that separate the five wave patterns are given by the following equations:

$$Q_{AB} = 1 \qquad \text{if } p_i \le p_o \le p_a, \tag{34}$$

$$Q_{AC_1} = 1 \qquad \text{if } p_a \le p_o \le p_b, \tag{35}$$

$$Q_{AC_2} = 1 \qquad \text{if } p_b \le p_o < \infty, \tag{36}$$

$$Q_{AD} = 1 \qquad \text{if } 0 \le p_o \le p_i, \tag{37}$$

$$Q_{BC_1} = \frac{2}{\gamma_i - 1}\left(\frac{p_o}{p_i}\right)^{\frac{\gamma_i - 1}{2\gamma_i}} - \frac{2}{\gamma_i - 1} \qquad \text{if } 0 \le p_o \le p_a, \tag{38}$$

$$Q_{C_1C_2} = Q_{BC_1} - \frac{a_o}{a_i} \qquad \text{if } 0 \le p_o \le p_b, \tag{39}$$

$$Q_{BD} = \frac{\gamma_i + 1}{\gamma_i - 1}\left(\frac{p_o}{p_i}\right)^{\frac{\gamma_i - 1}{2\gamma_i}} - \frac{2}{\gamma_i - 1} \qquad \text{if } 0 \le p_o \le p_i, \tag{40}$$

in which

$$p_a = p_i\left(\frac{\gamma_i + 1}{2}\right)^{\frac{2\gamma_i}{\gamma_i - 1}}$$

and

$$p_b = p_i\left(\frac{\gamma_i + 1}{2} + \frac{\gamma_i - 1}{2}\frac{a_o}{a_i}\right)^{\frac{2\gamma_i}{\gamma_i - 1}}.$$

Some of these boundaries depend not only on the Mach number Q and pressure ratio p_o/p_i but also the specific-heats ratio γ_i at the interior node and the sound speed ratio a_o/a_i, so the results in **Figure 10** are shown for the particular case of $\gamma_i = 7/5$ and $a_o/a_i = 6/5$.

The solutions for the boundary data for the wave patterns with subsonic and supersonic inflows and outflows can be obtained in algebraic form, and these solutions are summarized as follows:

$$p_e = \begin{cases} p_i & \text{for pattern A,} \\ p_o & \text{for B and C,} \\ p_i\left(\dfrac{2}{\gamma_i + 1} + \dfrac{\gamma_i - 1}{\gamma_i + 1}\dfrac{\lambda u_i}{a_i}\right)^{\frac{2\gamma_i}{\gamma_i - 1}} & \text{for D,} \end{cases} \tag{41}$$

$$u_e = u_i - \begin{cases} 0 & \text{for pattern A,} \\ \dfrac{2\lambda a_i}{\gamma_i - 1}\left(\dfrac{p_e}{p_i}\right)^{\frac{\gamma_i - 1}{2\gamma_i}} - \dfrac{2\lambda a_i}{\gamma_i - 1} & \text{for B, C and D,} \end{cases} \tag{42}$$

$$a_e = \begin{cases} a_i & \text{for pattern A,} \\ a_o & \text{for C,} \\ a_i\left(\dfrac{p_e}{p_i}\right)^{\frac{\gamma_i - 1}{2\gamma_i}} = a_i + \lambda\dfrac{\gamma_i - 1}{2}(u_i - u_e) & \text{for B and D,} \end{cases} \tag{43}$$

$$\rho_e = \begin{cases} \rho_i & \text{for pattern A,} \\ \rho_o & \text{for C,} \\ \rho_i\left(\dfrac{p_e}{p_i}\right)^{\frac{1}{\gamma_i}} & \text{for B and D,} \end{cases} \tag{44}$$

$$\gamma_e = \begin{cases} \gamma_i & \text{for patterns A, B and D} \\ \gamma_o & \text{for C,} \end{cases} \tag{45}$$

$$Re = \begin{cases} R_i & \text{for patterns A, B and D} \\ R_o & \text{for C.} \end{cases} \quad (46)$$

These solutions for the case with a compression wave are similar but somewhat simpler than those for the previous case with the shock wave, because the particular results for shock waves have been simplified to those for compression waves that fold directly into the results already obtained for rarefaction waves.

For computational methods that smear shock-front jumps over a few or many cells, the preceding boundary solution that approximates shock waves as compression waves should be quite adequate for prescribing boundary conditions at a grid end. However, in computational methods that treat strong shock jumps within a cell, such as some of Godunov's finite-volume methods and the random-choice method, the boundary solution in the preceding section that includes the shock jumps is recommended; the additional complexity is not overly burdensome.

Boundary Conditions for an Open Duct End

Many shock tubes, blast-wave simulators, wind tunnels and hypersonic impulse tunnels have test sections followed by a pipe extension with an end open to a large finite-volume reservoir or an effectively infinite-volume surrounding atmosphere. These facilities also sometimes use a high-pressure reservoir to produce the transient or steady flows inside the test section. The direction of an unsteady flow at the end of a duct open to the high-pressure reservoir or low-pressure atmosphere can be either outwards or inwards, depending on the flow properties of the gas in the duct and the state properties of the gas in the reservoir or atmosphere. Subsonic and supersonic duct outflows are normally produced by higher than atmospheric pressures inside the duct. These outflows typically separate from the duct end and form a subsonic or supersonic free jet in the surrounding reservoir or atmosphere. This jet eventually diffuses and dissipates from turbulent mixing with the surrounding reservoir or atmospheric gas. Duct inflows are normally produced by lower than atmospheric pressures inside the duct. The inflow at the duct entrance can be either subsonic or sonic, once again depending on the local flow conditions at the duct end and the properties of the surrounding gas in the reservoir or atmosphere. For duct entrance edges that are sharp, the inflow initially separates, incurs flow losses due to turbulent dissipation and eventually expands such that the inflow becomes more one-dimensional as it fills the duct cross-section.

In computations of one-dimensional unsteady flows in the aforementioned facilities, a convenient location to truncate the numerical grid is at the duct end open to a reservoir or an atmosphere. This avoids the difficulties of computing the complicated two-dimensional unsteady flow outside the duct in the surrounding reservoir or atmosphere. Nonetheless, the application of physically realistic boundary conditions is necessary to ensure that a one-dimensional calculation provides meaningful results. The boundary solutions for the open duct end which follow are an important step in this direction. Various boundary conditions for both the finite-volume reservoir and infinite-volume atmosphere are described in the next two sections, and a method for updating the thermodynamic properties of the gas in a finite-volume reservoir follows in the third section.

Wave Patterns and their Boundaries and Domains

In this boundary-solution method the boundary state $S(p_e, a_e, u_e, \gamma_e, R_e)$ at the open duct end is formulated on the basis of an extended Riemann problem that makes use of the gas state $S(p_o, a_o, u_o, \gamma_o, R_o)$ in the reservoir or atmosphere and the gas state $S(p_i, a_i, u_i, \gamma_i, R_i)$ at the interior node next to the open end. Unsteady flows inside the duct but near the open duct end are patched to steady inflows or outflows occurring in the adjacent reservoir or atmosphere to form what is called an 'extended' Riemann problem. These boundary flows and wave patterns that occur just inside and outside the open duct end are selected on the basis of physical compatibility and applicability and such that a comprehensive and unique solution S_e is obtainable for all possible states S_i and S_o.

For the general case of arbitrary states S_i and S_o, ten distinct types of flow or wave patterns for the open duct end have been identified and are considered for a complete analysis of the boundary conditions for the open duct end. These wave patterns are sketched in **Figure 11** for a duct with an open end on the right side, and they are labeled A, B, C, ..., J. The equivalent wave patterns for the other case of the left side of a grid with an open duct end are mirror images of those shown in **Figure 11**.

Patterns A and E do not contain any waves or a contact surface because the outflows for these patterns are supersonic and of sufficient speed that all waves are swept downstream and off the grid. Both patterns have supersonic free jets extending into the reservoir or atmosphere (not shown in **Figure 11**), and these patterns are different in that pattern A has an overexpanded supersonic jet that contains oblique shock waves (OSW) whereas the underexpanded jet associated with pattern E contains oblique rarefaction waves (ORW). Patterns B and G each have a single shock and rarefaction wave propagating into the duct with subsonic outflow at the duct end and an associated subsonic jet. Pattern F has a leftward moving rarefaction wave with outflow that is sonic with a supersonic jet containing oblique rarefaction waves, whereas pattern G with a rarefaction wave has a subsonic outflow and subsonic free jet. Patterns C and H feature shock and rarefaction waves but, in comparison to patterns B and G, they also contain an additional leftward moving contact surface with subsonic inflow at the duct end. In comparison to patterns C and H, patterns D and I have an additional rarefaction wave that propagates towards the duct end but is swept downstream into the duct. Furthermore, the inflow is sonic at the duct entrance and supersonic between the rarefaction wave (with its head fixed at the duct end) and the inward moving contact surface. Pattern J is similar to pattern I except that an additional vacuum region (V) exists between the gas originally in the duct and that entering from the

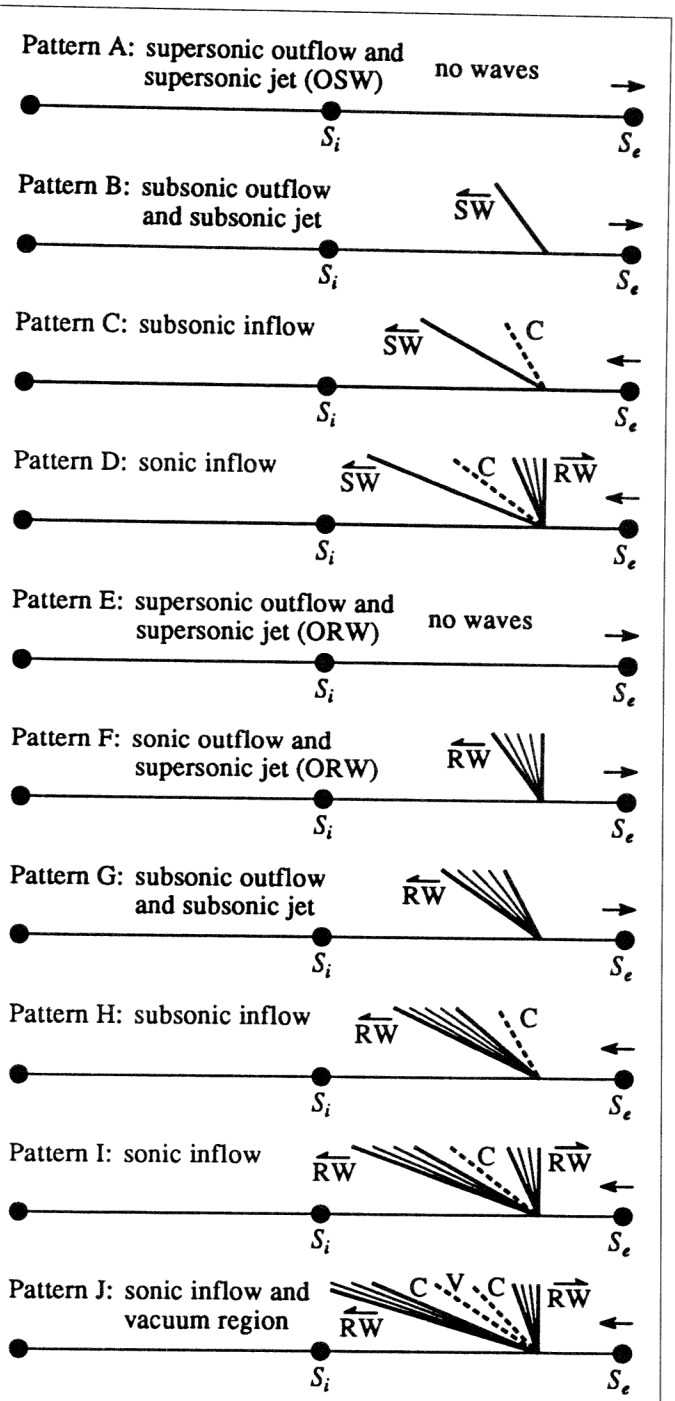

Figure 11.
Ten possible wave patterns for inflows and outflows at the right grid end for open-duct-end boundary conditions.

atmosphere.

The wave pattern and boundary solution for a particular boundary state S_e depends on the known interior state S_i and known reservoir state S_o. The starting point is the selection of the wave pattern dictated by states S_i and S_o, and this selection is facilitated by the map presented in **Figure 12** for the boundaries and domains of the ten wave patterns shown in **Figure 11**. In this map the pressure ratio p_o/p_i is plotted versus the Mach number $Q = \lambda u_i/a_i$, and Q includes the parameter λ so that the map summarizes boundaries for both right ($\lambda = +1$) and left

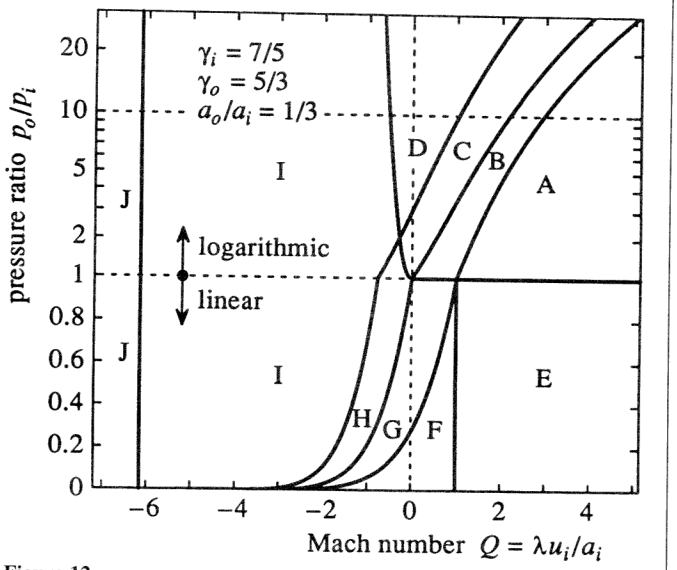

Figure 12.
Boundaries and domains of the ten possible wave patterns for open-duct-end boundary conditions.

($\lambda = -1$) grid ends. The twelve boundaries shown in **Figure 12** that demark the ten possible wave patterns are given algebraically as follows:

$$Q_{AB} = \sqrt{\frac{\gamma_i+1}{2\gamma_i}\frac{p_o}{p_i} + \frac{\gamma_i-1}{2\gamma_i}} \quad \text{if } p_o \geq p_i, \tag{47}$$

$$Q_{AE} \geq 1 \qquad \text{if } p_o = p_i\,, \tag{48}$$

$$Q_{BC} = \frac{\frac{p_o}{p_i}-1}{\gamma_i\sqrt{\frac{\gamma_i+1}{2\gamma_i}\frac{p_o}{p_a} + \frac{\gamma_i-1}{2\gamma_i}}} \quad \text{if } p_o \geq p_i, \tag{49}$$

$$0 \leq Q_{BG} \geq 1 \qquad \text{if } p_o = p_i\,, \tag{50}$$

$$Q_{CD} = \frac{\frac{p_o}{p_a}-1}{\gamma_i\sqrt{\frac{\gamma_i+1}{2\gamma_i}\frac{p_o}{p_a} + \frac{\gamma_i-1}{2\gamma_i}}} - \alpha \quad \text{if } p_o \geq p_a, \tag{51}$$

$$Q_{CH} = -\alpha\sqrt{\frac{\gamma_o+1}{\gamma_o-1} - \frac{\gamma_o+1}{\gamma_o-1}\left(\frac{p_i}{p_o}\right)^{\frac{\gamma_o-1}{\gamma_o}}} \quad \text{if } p_i \leq p_o \leq p_a, \tag{52}$$

$$Q_{DI} = \frac{\gamma_o+1}{\gamma_o-1}\,\alpha\left[\sqrt{\frac{2}{\gamma_o+1}\left(\frac{p_i}{p_o}\right)^{\frac{\gamma_o-1}{2\gamma_o}} - 1}\right] \quad \text{if } p_o \geq p_a, \tag{53}$$

$$Q_{EF} = 1 \qquad \text{if } 0 \leq p_o \leq p_i, \tag{54}$$

$$Q_{FG} = \frac{\gamma_i+1}{\gamma_i-1}\left(\frac{p_o}{p_i}\right)^{\frac{\gamma_i-1}{2\gamma_i}} - \frac{2}{\gamma_i-1} \quad \text{if } 0 \leq p_o \leq p_i, \tag{55}$$

$$Q_{GH} = \frac{2}{\gamma_i - 1}\left(\frac{p_o}{p_i}\right)^{\frac{\gamma_i - 1}{2\gamma_i}} - \frac{2}{\gamma_i - 1} \quad \text{if } 0 \le p_o \le p_i, \tag{56}$$

$$Q_{HI} = \frac{2}{\gamma_i - 1}\left(\frac{p_o}{p_a}\right)^{\frac{\gamma_i - 1}{2\gamma_i}} - \frac{2}{\gamma_i - 1} - \alpha \text{ if } 0 \le p_o \le p_a, \tag{57}$$

$$Q_{IJ} = -\frac{2}{\gamma_i - 1} - \frac{\gamma_o + 1}{\gamma_o - 1}\alpha \text{ if } p_o \ge 0, \tag{58}$$

in which $p_a = p_i\left(\frac{\gamma_o + 1}{2}\right)^{\gamma_o/(\gamma_o - 1)}$, $Q = \lambda u_i/a_i$, and $\alpha = \sqrt{\frac{2}{\gamma_o + 1}}\frac{a_o}{a_i}$.

These equations are all derived on the basis of those for rarefaction waves, shock waves, contact surfaces and quasi-steady isentropic flows (Equations 3 - 10) in combination with additional information concerning the various wave patterns. Some of these boundaries depend not only on the Mach number Q and pressure ratio p_o/p_i but also the specific-heats ratios γ_i and γ_o and the sound-speed ratio a_o/a_i, so the results in **Figure 12** are shown for the particular case of $\gamma_o = 7/5$, $\gamma_i = 5/3$ and $a_o/a_i = 1/3$.

The wave patterns on either side of any boundary have a common limiting pattern; in other words, the domains merge smoothly at their common boundary. For example, consider patterns B and C and their common boundary. Pattern B has a single shock and outflow, whereas pattern C has a shock, contact surface and inflow. At their common boundary the outflow and inflow reduce to no flow and the strength of the shock in both patterns becomes equal. As another example, consider patterns C and H and their common boundary. Pattern C has an inward moving shock and pattern H has an inward moving rarefaction wave, and in both cases these waves are followed by a contact surface with inflow from the atmosphere. At their common boundary the contact surface and inflow still occur but in both cases the inward moving wave degenerates to a Mach wave.

Some additional observations about the boundaries between various wave patterns in **Figure 12** are made. The confluence point for patterns C, D, I and H has the pressure coordinate $p_a = p_i\left(\frac{\gamma_o + 1}{2}\right)^{\gamma_o/(\gamma_o - 1)}$ and Mach-number coordinate $Q = \sqrt{\frac{2}{\gamma_o + 1}}\frac{a_o}{a_i}$. The boundary between patterns F and G converges to the boundary between patterns G and H as p_o/p_i approaches zero, and this limiting value is given by $Q = -\frac{2}{\gamma_i - 1}$. The limiting value for the boundary between patterns H and I as p_o/p_i approaches zero is given by $Q = -\sqrt{\frac{2}{\gamma_o + 1}}\frac{a_o}{a_i} - \frac{2}{\gamma_i - 1}$, which lies between the previous limiting value and the boundary between patterns I and J. Hence, the boundaries between patterns F and G, G and H, and H and I are distinct and do not cross. The boundary between patterns D and I is asymptotic to the vertical line $Q = -\frac{\gamma_o + 1}{\gamma_o - 1}\sqrt{\frac{2}{\gamma_o + 1}}\frac{a_o}{a_i}$, which always lies between the boundary for patterns C and D and that for patterns I and J. Further inspection reveals that the domains of the ten possible wave patterns cover the entire pressure versus flow-velocity diagram for all physically meaningful values of p_o/p_i and Q, without gaps or overlap. Hence, unique solutions for these wave patterns and boundary data S_e always exist for the general case of arbitrary states S_i and S_o. In addition, the solution state S_e depends on only five non-dimensional parameters: p_o/p_i, $Q = \lambda u_i/a_i$, γ_o, γ_i and a_o/a_i.

Boundary Data Solutions

The boundary solution for wave patterns A and E for the open duct end are considered first. Both wave patterns have supersonic outflow and no waves, although the supersonic free jets outside the duct are different. The boundary solution for state S_e is given obviously by

$$p_e = p_i,\ a_e = a_i,\ \rho_e = \rho_i,\ u_e = u_i,\ \gamma_e = \gamma_i,\ R_e = R_i, \tag{59}$$

or more simply $S_e = S_i$, for both wave patterns A and E.

For wave pattern B, a weak shock wave travels into the duct and leaves outflow that is subsonic (with an associated subsonic free jet). In this boundary solution the pressure in the free jet is assumed equal to that of the surrounding reservoir or atmosphere. By setting the duct end pressure p_e equal to the reservoir or atmospheric pressure p_o, the strength of the shock wave and thereby the boundary data can be obtained by using Equations 3 to 5 for shock waves. The results are

$$u_e = u_i - \lambda a_i \frac{\frac{p_o}{p_i} - 1}{\gamma_i\sqrt{\frac{\gamma_i + 1}{2\gamma_i}\frac{p_o}{p_i} + \frac{\gamma_i - 1}{2\gamma_i}}},$$

$$a_e = a_i \sqrt{\frac{(\gamma_i - 1)(p_o/p_i) + (\gamma_i + 1)}{(\gamma_i - 1)(p_i/p_o) + (\gamma_i + 1)}}, \tag{60}$$

$$\rho_e = \rho_i \frac{(\gamma_i + 1)(p_o/p_i) + (\gamma_i - 1)}{(\gamma_i - 1)(p_o/p_i) + (\gamma_i + 1)},$$

$$p_e = p_o,\ \gamma_e = \gamma_i,\ R_e = R_i,$$

for wave pattern B.

For wave patterns D, I and J the inflow starts from the stagnation state of the atmosphere and accelerates to sonic or choked inflow at the duct entrance (i.e., $M_e = -\lambda$). This information combined with Equations 9 and 10 for steady flows results in the boundary solution given by

$$p_e = p_o\left(\frac{2}{\gamma_o + 1}\right)^{\frac{\gamma_o}{\gamma_o - 1}},\ \rho_e = \rho_o\left(\frac{2}{\gamma_o + 1}\right)^{\frac{1}{\gamma_o - 1}},$$

$$u_e = -\lambda a_o \sqrt{\frac{2}{\gamma_o+1}}, \quad a_e = a_o \sqrt{\frac{2}{\gamma_o+1}},$$

$$\gamma_e = \gamma_o, R_e = R_o, \tag{61}$$

for wave patterns D, I and J.

For wave pattern F, the inward moving rarefaction wave accelerates the outflow to a sonic velocity at the duct end (i.e., $M_e = \lambda$). This information along with Equations 7 and 8 for rarefaction waves results in the boundary solution given by

$$p_e = p_i \beta^{\frac{2\gamma_i}{\gamma_i-1}}, \quad \rho_e = \rho_i \beta^{\frac{2}{\gamma_i-1}},$$

$$u_e = \lambda a_i \beta, a_e = a_i \beta, \gamma_e = \gamma_i, R_e = R_i, \tag{62}$$

for wave pattern F, in which $\beta = \frac{2}{\gamma_i+1} + \frac{\gamma_i-1}{\gamma_i+1} Q$ and $Q = \lambda u_i / a_i$.

For wave pattern G, the outflow and free jet are both subsonic, and the atmospheric and free-jet pressures are essentially equal (i.e., $p_e = p_o$). This information, along with Equations 7 and 8 for rarefaction waves, yields the boundary solution given by

$$u_e = u_i + \frac{2\lambda a_i}{\gamma_i - 1}\left[1 - \left(\frac{p_o}{p_i}\right)^{\frac{\gamma_i-1}{2\gamma_i}}\right],$$

$$a_e = a_i \left(\frac{p_o}{p_i}\right)^{\frac{\gamma_i-1}{2\gamma_i}}, \quad \rho_e = \rho_i \left(\frac{p_o}{p_i}\right)^{\frac{1}{\gamma_i}},$$

$$p_e = p_o, \gamma_e = \gamma i, R_e = R_i, \tag{63}$$

for pattern G.

Now consider the similar but more complicated cases of boundary conditions for patterns C and H. The equations for the flow across the leftward moving shock wave (Equations 3 - 5) and rarefaction wave (Equations 7 and 8) in patterns C and H, respectively, can be combined with the steady subsonic duct inflow from the reservoir or atmosphere (Equations 9 and 10) into one non-linear algebraic expression for the unknown pressure ratio $Z = p_e/p_o$. For wave pattern C, the resulting expression is given by

$$\frac{2}{\gamma_o - 1}\frac{a_o^2}{a_i^2}\left[1 - Z^{\frac{\gamma_o-1}{\gamma_o}}\right] = \left[Q - \frac{\frac{p_o}{p_i}Z - 1}{\gamma_i \sqrt{\frac{\gamma_i+1}{2\gamma_i}\frac{p_o}{p_i}Z + \frac{\gamma_i-1}{2\gamma_i}}}\right]^2, \tag{64}$$

and for the case of wave pattern H, the resulting expression is

$$\frac{2}{\gamma_o - 1}\frac{a_o^2}{a_i^2}\left[1 - Z^{\frac{\gamma_o-1}{\gamma_o}}\right] = \left[Q + \frac{2}{\gamma_i - 1} - \frac{2}{\gamma_i - 1}\left(\frac{p_o}{p_i}Z\right)^{\frac{\gamma_i-1}{2\gamma_i}}\right]^2. \tag{65}$$

The solution for Z from either expression can be obtained by using a Newton iterative procedure. An initial estimate for Z is selected, a residual denoted by $F(Z)$ is computed, and successively improved estimates for Z are then given by $Z_{j+1} = Z_j - F(Z_j)/F'(Z_j)$, in which $F'(Z) = dF/dZ$. A practical initial estimate for the value of Z that has the correct upper and lower bounds is given by

$$Z = \begin{cases} Z_{BC} + (Z_{CH} - Z_{BC})\dfrac{Q - Q_{BC}}{Q_{CH} - Q_{BC}} & \text{if } p_i \le p_o \le p_a, \\ Z_{BC} + (Z_{CD} - Z_{BC})\dfrac{Q - Q_{BC}}{Q_{CD} - Q_{BC}} & \text{if } p_o \ge p_a, \end{cases} \tag{66}$$

for the specific case of pattern C, and the corresponding practical initial estimate for wave pattern H follows as

$$Z = \begin{cases} Z_{HI} + (Z_{GH} - Z_{HI})\dfrac{Q - Q_{HI}}{Q_{GH} - Q_{HI}} & \text{if } 0 \le p_o \le p_i, \\ Z_{HI} + (Z_{CH} - Z_{HI})\dfrac{Q - Q_{HI}}{Q_{CH} - Q_{HI}} & \text{if } p_i \le p_o \le p_a, \end{cases} \tag{67}$$

in which Q_{BC}, Q_{CD}, Q_{CH}, Q_{GH} and Q_{HI} are Mach numbers for the pattern boundaries given earlier by Equations 47 - 58,

$$Z_{BC} = Z_{GH} = 1, Z_{CH} = Z_{GH} = \frac{pi}{po}, Z_{CD} = Z_{HI} = \left(\frac{2}{\gamma_o+1}\right)^{\gamma_o/(\gamma_o-1)}$$

are pressure ratios corresponding to the respective boundaries, and $p_a = p_i\left(\frac{\gamma_o+1}{2}\right)^{\gamma_o/(\gamma_o-1)}$. Once a value of Z is known, the boundary solution can be expressed as

$$p_e = p_o Z, \quad a_e = a_o Z^{\frac{\gamma_o-1}{2\gamma_o}},$$

$$u_e = -\lambda a_o \sqrt{\frac{2}{\gamma_o - 1}\left(1 - Z^{\frac{\gamma_o-1}{\gamma_o}}\right)}, \tag{68}$$

$$\rho_e = \rho_o Z^{\frac{1}{\gamma_o}}, \gamma_e = \gamma_o, R_e = R_o,$$

for both wave patterns C and H.

For the specific but frequently encountered case when $\gamma_i = \gamma_o = \gamma$ for pattern H, the non-linear algebraic expression given by Equation 65 simplifies to the standard quadratic form $aX^2 - 2bX - c = 0$. In this case an implicit solution for Z can be obtained as

$$a = \frac{\gamma-1}{2}\frac{a_o^2}{a_i^2} + \left(\frac{p_o}{p_i}\right)^{\frac{\gamma-1}{\gamma}},$$

$$b = (1 + \frac{\gamma-1}{2} Q)\left(\frac{p_o}{p_i}\right)^{\frac{\gamma-1}{2\gamma}},$$

$$c = \frac{\gamma-1}{2} \frac{a_o^2}{a_i^2} - \left(1 + \frac{\gamma-1}{2} Q\right)^2, \tag{69}$$

$$Z = X^{\frac{2\gamma}{\gamma-1}} = \left(\frac{b}{a} + \sqrt{\frac{b^2}{a^2} + \frac{c}{a}}\right)^{\frac{2\gamma}{\gamma-1}}.$$

When applicable this solution can be used to avoid the iterative solution procedure for Z as defined by Equation 65 for pattern H. There appears to be no equivalent non-iterative solution available for Equation 64 for wave pattern C.

Properties of the Gas in a Finite-Volume Reservoir

The finite-volume reservoir is considered attached to a duct at the open end such that a gas flow can occur from the duct to the reservoir or conversely, depending on the open-duct-end boundary solution using the states of the gases in both the duct and reservoir. The state of the gas in the reservoir is denoted by $S(p_o, a_o, u_o = 0, \gamma_o, R_o)$, for which the average gas velocity in the reservoir is assumed to be zero. As gas flows into or out of the reservoir via the open duct end, the state of the reservoir gas will change with time because of the gain or loss of mass and energy. If the gas flowing into the reservoir differs from that in the reservoir, then the mixing of these different gases also occurs in the reservoir and γ_o and R_o change with time. The update of the gas properties for a finite-volume reservoir is considered herein.

The state $S(p_e, a_e, u_e, \gamma_e, R_e)$ of the gas at the open duct end is considered known at some time t, or the j^{th} time level t^j, being determined by the application of open-duct-end boundary conditions set out in the last section. This duct end state S_e is assumed constant over the short time period $\Delta t = t^{j+1} - t^j$, and the mass per unit of reservoir volume that flows into or out of the reservoir during this time period is given by

$$\Delta\rho_o^j = \lambda \frac{\rho_e^j u_e^j A \Delta t}{V}, \tag{70}$$

in which A and V are the duct area and reservoir volume, respectively, $\lambda = +1$ for a reservoir at the right end of the computational domain and $\lambda = -1$ for the opposite case. This change in reservoir mass per unit of reservoir volume is the key element in the temporal update of the properties of the reservoir gas.

The state of the gas in the reservoir can be updated in time by considering a control volume around the reservoir and implementing a conventional control-volume analysis for the conservation of mass and energy, and also including thermally perfect gas mixing rules for the general case of different reservoir and duct gases. The results can be summarized as follows:

$$\rho_o^{j+1} = \rho_o^j + \Delta\rho_o^j,\ u_o^{j+1} = u_o^j = 0,$$

$$R_o^{j+1} = R_o^j + \frac{\Delta\rho_o^j}{\rho_o^j + \Delta\rho_o^j}(R_e^j - R_o^j),$$

$$\gamma_o^{j+1} = \gamma_o^j + \frac{\frac{1}{\gamma_e^j - 1} R_e^j \Delta\rho_o^j}{\frac{1}{\gamma_o^j - 1} R_o^j \rho_o^j + \frac{1}{\gamma_e^j - 1} R_e^j \Delta\rho_o^j}(\gamma_e^j - \gamma_o^j), \tag{71}$$

$$p_o^{j+1} = \frac{\gamma_o^{j+1} - 1}{\gamma_o^j - 1} p_o^j + \frac{\gamma_o^{j+1} - 1}{\gamma_e^j - 1}\left[(a_e^2)^j + \frac{\gamma_e^j - 1}{2}(u_e^2)^j\right]\Delta\rho_o^j,$$

$$a_o^{j+1} = \sqrt{\gamma_o^{j+1} p_o^{j+1}/\rho_o^{j+1}},$$

for both cases of reservoir inflows and outflows. The effects of the mixing of different reservoir and duct gases vanish conveniently when $\gamma_e = \gamma_o$ and $R_e = R_o$. This occurs as expected for the cases of identical reservoir and duct gases and also as required for the case of flows out of the reservoir.

Terms for heat transfer between the reservoir gas and walls are not included in the mass and energy balances leading to Equations 71 because the heat-transfer coefficient is strongly dependent on the reservoir geometry and physical orientation, as well as the degree of forced convection from the free jet for the case of duct flows into the reservoir. These heat-transfer effects must be added by the user if they are required. Note, however, that the effects of heat transfer in the reservoirs of shock tubes, hypersonic impulse tunnels, and most blast simulators normally are not important owing to the short duration of flows therein.

Numerical Examples

Some numerical examples are presented in this section to demonstrate the applicability and usefulness of the solutions for various boundary conditions given in previous sections. Five examples are presented for the case of one-dimensional non-stationary gas flows and one example is given for a two-dimensional steady flow.

One-Dimensional Flow Problems

Five initial boundary-value problems for the system of equations given by Equations 1 and 2 are considered and numerical results are presented for three different solution schemes. These schemes are the random-choice method (RCM) with a quasi-random solution sampling sequence, the first-order Godunov method, and the higher-order total-variation-diminishing (TVD) flux-differencing scheme of Roe with a combination of van Leer and 'superbee' flux limiters. Details of these three explicit time-stepping solution algorithms are available from Godunov (1959), Glimm (1965), Roe (1981), Roe and Pike (1984), Sweby (1984), and Gottlieb [illegible]. In all examples the gas flow consists of air ($\gamma = 7/5$, $R =$ [illegible] $J/kg\bullet K$), the grids are spatially uniform, and the time [illegible] chosen such that the appropriate Courant-Friedrichs-Le[illegible]) condition is satisfied. These numerical predictions are al[illegible]pared to exact analytical solutions when possible.

The first example consists of the reflection of a moving shock wave from the closed end of a duct on the right side of a numerical grid. This problem is used to test the closed-end boundary solutions. At time $t = 0$ ms a rightward moving shock wave of constant strength is located at $x = 5$ m on a grid with 141 nodes extending from x equal to 0 to 10 m. This shock is moving into quiescent air at an initial pressure of 101.1 kPa and temperature of 300.0 K, and the initial shock Mach number M_s is 5 and the associated pressure ratio is 29 (pressure of 2.932 MPa behind the shock). Three numerical predictions and the exact analytical solution are given in the form of spatial distributions of pressure in **Figure 13**, showing the shock wave motion prior to and after reflection from the closed end. The incident shock is shown at the time $t = 2$ ms during its motion toward the closed end located at $x = 10$ m. The reflected shock wave with a new strength of $M_s = -2.408$ and pressure ratio of 6.600 (final pressure of 19.35 MPa) is shown at a later time of $t = 12$ ms. These results illustrate clearly that the reflection process is well resolved by all three numerical procedures and that the Dirichlet boundary solution for the closed end performs well for these numerical methods. Companion tests involving the reflection of a rarefaction wave from the closed end resulted in similar conclusions.

The second example consists of a shock-tube problem similar to the initial value problem considered by Hedstrom (1979). This problem is used to test the non-reflecting boundary solution. These are tested at both ends of the numerical grid with 201 nodes extending from x equal 0 to 10 m. The initial discontinuity at $t = 0$ ms is located at $x = 3$ m and has pressure and density ratios p_{left}/p_{right} and ρ_{left}/ρ_{right} equal to 10. The air is initially quiescent with other initial conditions given by $p_{left} = 101.1$ kPa, $T_{left} = T_{right} = 300$ K and $\rho_{left} = 1.174$ kg/m^3. The discontinuity at time $t = 0$ ms breaks into a growing self-similar wave pattern consisting of a rarefaction wave propagating to the left and a shock wave followed by a contact surface travelling to the right. The pressure ratio $p^*_{left}/p_{left} = p^*_{right}/p_{left}$ and flow velocity ratio $u^*_{left}/a_{left} = u^*_{right}/a_{left}$ for the interior states of wave patterns on each side of the contact surface are given by 2.848 and 0.8212, respectively, and the two intermediate flow Mach numbers M^*_{left} and M^*_{right} are equal to 0.9826 and 0.6958 (both subsonic).

Three numerical predictions and the exact solution to this shock-tube problem are shown in **Figure 14**, in the form of spatial distributions of density at three different time levels. At $t = 6$ ms the shock wave, contact surface and rarefaction waves are all within the computational grid. At $t = 15$ ms the shock wave and first half of the rarefaction wave have left opposite sides of the grid via the two non-reflecting boundaries at x equal to 0 and 10 m. By $t = 30$ ms the contact surface has also moved off the grid, and so has about three-quarters of the rarefaction wave. Because the tail of the rarefaction wave is almost stationary ($u^*_{right} - a^*_{right} = -0.0146\, a_{left}$), its motion is not noticeable in 30 ms. From the three numerical predictions and the exact solution, one can observe that the shock wave, contact surface and fan of the rarefaction wave are transmitted through the right and left boundaries with no noticeable reflections. This is also true for the cases of other variables such as the pressure, sound speed and flow velocity. Clearly, the non-reflecting boundary solutions perform well for all three numerical procedures.

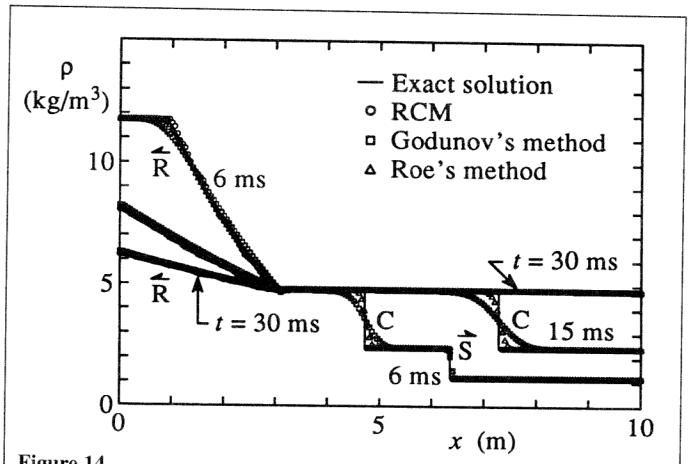

Figure 14.
Shock-tube problem with non-reflecting boundaries at $x = 0$ m and $x = 10$ m (for an initial pressure ratio $p_{left}/p_{right} = 10$).

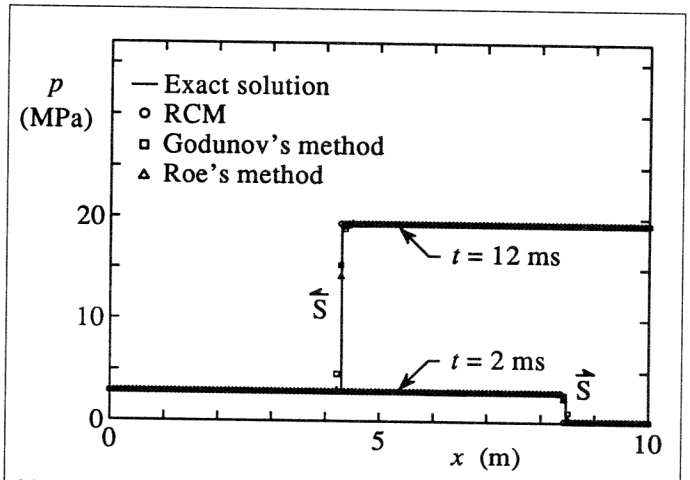

Figure 13.
Reflection of a shock wave ($M_s = 5$) from a closed-end boundary located at $x = 10$ m.

The third example consists of a shock wave incident on the end of a duct open to the atmosphere (on the right side of the numerical grid). This problem is used to test one of the ten open-duct-end boundary solutions. At time $t = 0$ ms a rightward moving shock wave of constant strength passes the location $x = 5$ m on a grid with 201 nodes and extending from x equal to 0 to 10 m. This shock is again moving into stagnant air with pre-shock conditions given by 101.1 kPa, 300 K and 1.174 kg/m^3, and these are also the stagnation properties of the surrounding atmosphere (p_o, T_o and ρ_o). The initial shock Mach number M_s is 1.5 with a post-shock pressure and density of 2.458 p_o and 1.862 ρ_o, and the flow induced by the shock is subsonic ($M = 0.6044$). The passage of the shock out of the open duct end produces a reflected rarefaction wave that is centered (at $x = 10$ m) and yields sonic outflow with a supersonic free jet in the atmosphere. Exact flow conditions at the duct exit are given as $u_e = a_e = 1.073 a_o$, $p_e = 1.525\, p_o$ and $\rho_e = 1.324\, \rho_o$, after the shock leaves the duct.

Three numerical predictions and the exact solution are shown in the form of spatial distributions of density in **Figure 15**, at three different times. The incident shock is still in the computational domain at the time $t = 7$ ms during its motion towards the open duct end at $x = 10$ m. At the later times of 30 and 45 ms, the shock is no longer present and the reflected rarefaction wave spreads farther into the grid (with the tail stationary or vertical at $x = 10$ m). It is clear from these results that this open-duct-end boundary solution works well in conjunction with the RCM and the Godunov and Roe numerical schemes, providing an accurate representation of the shock-induced flow field in the vicinity of the open duct end (even though Godunov's results are rather smeared through the head of the rarefaction wave).

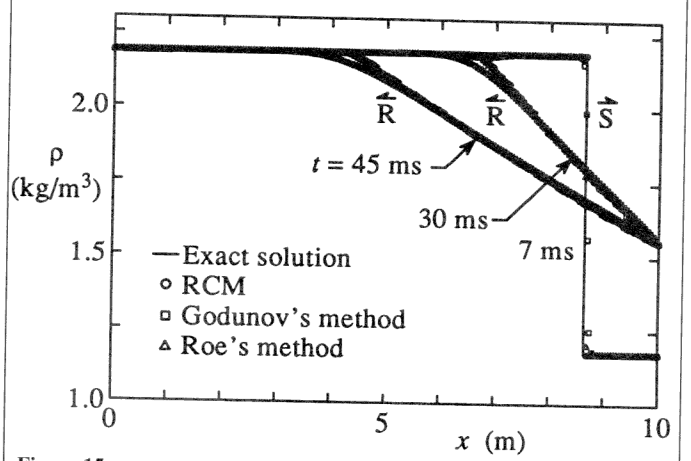

Figure 15.
Shock wave ($M_S = 1.5$) encountering an open-duct-end boundary located at $x = 10$ m.

The fourth example is a rarefaction wave incident on the end of a duct open to the atmosphere (on the left side of the numerical grid). This problem is used to test another one of the ten open-duct-end boundary solutions. At time $t = 0$ ms a leftward moving rarefaction wave is produced as a discontinuity at the location $x = 5$ m on a grid with 201 nodes and extending from x equal to 0 to 10 m. The initial conditions of the atmosphere and the air on both sides of the discontinuity are $p_o = p_{\text{left}} = 101.1$ kPa, $a_o = a_{\text{left}} = 347.2$ m/s, $M_{\text{left}} = -1.008$, $p_{\text{right}} = 0.2848\,p_o$, $a_{\text{right}} = 0.8358\,a_o$, and $M_{\text{right}} = -0.2235$. This rarefaction wave propagates to the left and leaves via the open-duct-end boundary at $x = 0$ m, producing a transient inflow from the atmosphere that is headed by a shock wave that is becoming stronger. This inflow eventually becomes quasi-steady with the asymptotic flow conditions given by $p^* = 0.8271\,p_o$, $a^* = 0.9732\,a_o$ and $M^* = 0.5379$, and the shock Mach number M_S approaches asymptotically the value of 1.622. There is no analytical solution for the transient flow development leading to the final quasi-steady flow conditions.

Numerical solutions for this problem using the RCM and Godunov and Roe's schemes are depicted in **Figure 16**, in which spatial distributions of pressure are depicted. At $t = 5$ ms the leftward moving expansion wave is still entirely within the

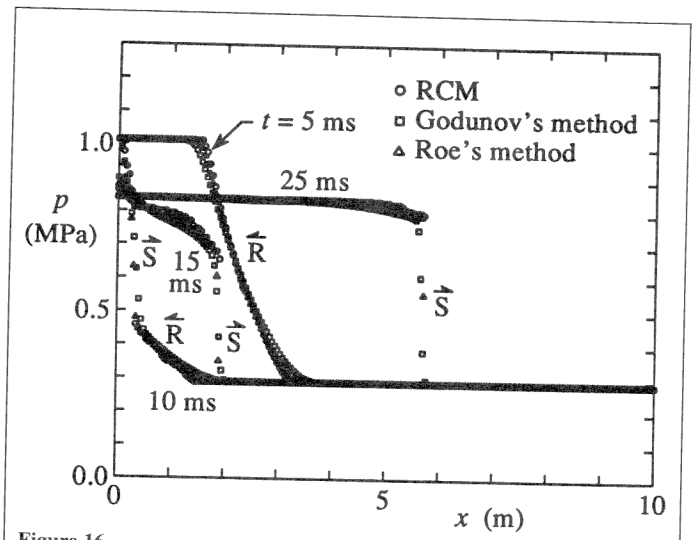

Figure 16.
Rarefaction wave ($p_{left}/p_{right} = 0.2848$) encountering an open-duct-end boundary located at $x = 0$ m.

computational domain. At $t = 10$ ms, about half of the rarefaction wave has left the grid and a rightward moving compression wave that steepens into a shock wave has developed next to the open end. At the later times of 15 and 25 ms this shock wave moves successively farther into the computational domain and becomes stronger. At $t = 25$ ms the inflow has nearly reached the quasi-steady Mach number of 0.5379 (within 3%), but the shock front requires a much longer time to approach its quasi-steady strength. Nonetheless, it is apparent that the open-duct-end boundary solution performs well in all three computational methods for predicting the transient flow development in the vicinity of the open end.

The fifth example consists of the flow of air from a high-pressure reservoir (700.0 kPa, 4.877 kg/m³, 500 K) on the left side of the grid to a low-pressure reservoir (229.81 kPa, 1.601 kg/m³, 500 K) on the right side of the grid through a convergent-divergent duct (de Laval nozzle). This problem is used to further test open-end boundary solutions. The upstream and downstream reservoirs are both infinitely large with constant state properties, the duct connecting the two reservoirs has a symmetric area distribution given by

$$A(x) = \begin{cases} A_o & 0 \text{ m} \le x < 1 \text{ m}, \\ A_o \sqrt{\dfrac{A_t}{A_o}} \exp\left[\ln\left(\sqrt{\dfrac{A_o}{A_t}}\right)\cos\left(\dfrac{\pi(x-1)}{4}\right)\right] & 1 \text{ m} \le x \le 9 \text{ m}, \\ A_o\,, & 9 \text{ m} < x \le 10 \text{ m}, \end{cases} \quad (72)$$

in which $A_o = 11.9A_t$ is the area at both the upstream and downstream reservoirs and $A_t = 1$ m² is the minimum area at the nozzle throat ($x = 5$ m). At time $t = 0$ ms the properties of each reservoir are extended into the duct to the throat location at $x = 5$ m, forming an initial discontinuity in pressure and density (ratio of 3.046), from which the flow computations are initiated. As time increases the unsteady nozzle flow decays to a steady flow. This steady flow has a duct inlet pressure of 698.8 kPa and Mach number 0.4869, sonic flow at the throat ($M_t = 1.0$),

supersonic flow from the throat to an upstream-facing recompression shock with $M_s = 3.0$ at $x = 7.212$ m, and subsonic flow thereafter to an outlet pressure of 229.8 kPa and Mach number of 0.1501, respectively. The free jet in the low-pressure reservoir is subsonic.

Numerical results from the RCM and Godunov and Roe's schemes are shown along with the exact steady-flow solution in **Figure 17**, for the case of 201 nodes over the range $0 \leq x \leq 10$. The density distributions at the initial time $t = 0$ ms and after a long time of 2000 ms are both shown. In the latter case, the three different numerical predictions agree well with the steady-state solution. Owing to the nondissipative nature of the RCM and small perturbations introduced by operator-splitting corrections for source terms involving the duct area variation, a few small-amplitude transient disturbances persist in its solution. Nevertheless, these results further demonstrate the applicability and validity of the boundary solutions for the open duct end.

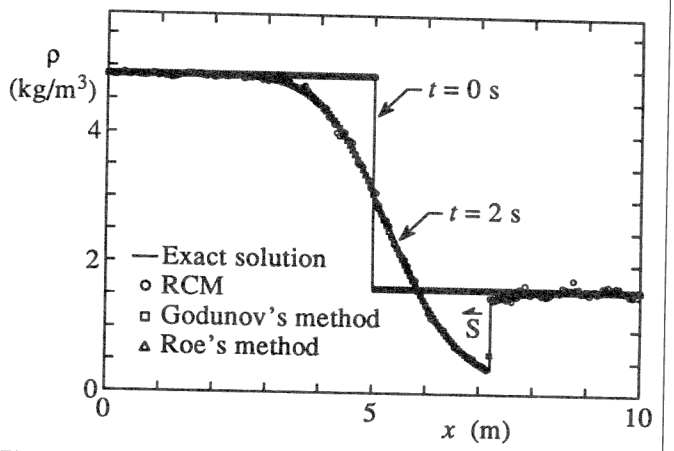

Figure 17.
Flow from one reservoir to another via a de Laval convergent-divergent nozzle with open-duct-end boundaries located at $x = 0$ m and $x = 10$ m (for a reservoir pressure ratio $p_{left}/p_{right} = 3.05$).

Two-Dimensional Flow Problem

The possibility of using the preceding boundary solutions for multi-dimensional flow predictions is demonstrated by solving one problem involving the steady two-dimensional planar flow of air ($\gamma = 7/5$, $R = 287.06$ J/kg•K) through a channel with a reverse-flow-angled orifice (depicted in **Figure 18**). In this problem, air flows from right to left through the orifice and into a stagnant atmosphere. The flow in the atmosphere is in the form of a free jet. The atmospheric pressure, temperature, and sound speed of the quiescent air outside the orifice are $p_o = 100$ kPa, $T_o = 287.65$, and $a_o = 340$ m/s. The half-widths of the channel and orifice are 8.89 and 2.54 cm, respectively, and the acute angle between the straight channel and orifice-plate walls is 50 degrees. The initial or upstream flow conditions of the air in the channel are set to $p_\infty = 125$ kPa, $T_\infty = 287.65$, and $a_\infty = 340$ m/s.

The channel flow is assumed to be both compressible and inviscid, and therefore it is assumed to be governed by the two-dimensional form of the inviscid equations of gas dynamics, which can be expressed as

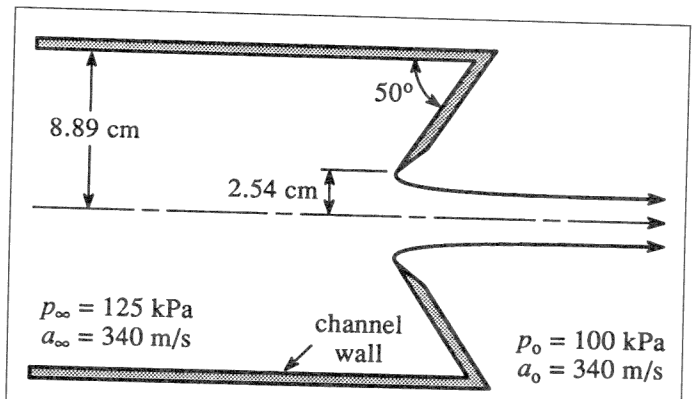

Figure 18.
Duct geometry for a steady two-dimensional subsonic flow with a free jet.

$$\frac{\partial}{\partial t}[U] + \frac{\partial}{\partial x}[F(U)] + \frac{\partial}{\partial y}[G(U)] = 0 , \tag{73}$$

where

$$U = \begin{bmatrix} \rho \\ \rho u \\ \rho v \\ \rho\left(\epsilon + \frac{1}{2}(u^2+v^2)\right) \end{bmatrix}, \tag{74}$$

$$F = \begin{bmatrix} \rho u \\ \rho u^2 + p \\ \rho uv \\ \rho u\left(\epsilon + \frac{p}{\rho} + \frac{1}{2}(u^2+v^2)\right) \end{bmatrix},$$

$$G = \begin{bmatrix} \rho v \\ \rho uv \\ \rho u^2 + p \\ \rho v\left(\epsilon + \frac{p}{\rho} + \frac{1}{2}(u^2+v^2)\right) \end{bmatrix}. \tag{75}$$

In these expressions, v is the component of the flow velocity in the y-coordinate direction. A first-order dimension-split version of Roe's upwind finite-volume scheme was used to solve the preceding equations for this duct and free-jet flow problem. A time-marching procedure is used to advance the solution to steady state on a logically rectangular 220 by 72 curvilinear computational mesh. Further details about the two-dimensional solution algorithm are available from Groth (1993).

In order to solve this problem on a finite solution domain, three of the one-dimensional boundary solutions developed

herein were utilized. For each, the flow was assumed to be locally one-dimensional in the direction normal to the boundary. The reflecting boundary conditions described above were used in conjunction with the additional condition of flow tangency to prescribe boundary data at the solid walls of the channel and orifice, as well as along the axis of symmetry. The prescribed subsonic inflow boundary conditions (along with the condition that the flow is purely axial) were used to specify the upstream boundary conditions at the channel inlet with $p_o = p_\infty = 125$ kPa and $a_o = a_\infty = 340$ m/s. Finally, open end boundary conditions at an infinite reservoir described in the previous section with $p_o = 100$ kPa and $a_o = 340$ m/s were used to specify flow conditions at the artificially truncated boundaries downstream of the orifice.

The numerical solution of the two-dimensional flow field is presented in **Figures 19** and **20**. Contours of constant flow speeds and flow streamlines are shown. The convergence of the flow through the orifice and subsequent formation of the subsonic free jet are shown in the two figures. For the finite solution domain considered herein, the specification of upstream and downstream boundary conditions make this a challenging problem to solve by numerical methods, and it should be apparent from the predicted results that the one-dimensional boundary solutions for the reflecting, prescribed subsonic inflow, and open end boundaries permit a fairly accurate computation of this two-dimensional flow. In particular, the streamlines forming the subsonic jet are straight (aligned with the axis of symmetry), the pressure in the jet is essentially constant and equal to the atmospheric pressure, p_o, and the jet leaves the computational domain cleanly without creating spurious solution errors in the vicinity of the downstream boundary. Note that there is some evidence of the formation of a numerical boundary layer near the channel walls and axis of symmetry, as evident in the contour plot of **Figure 19**. Such features are inherent to all first-order dimension-split calculations of this type.

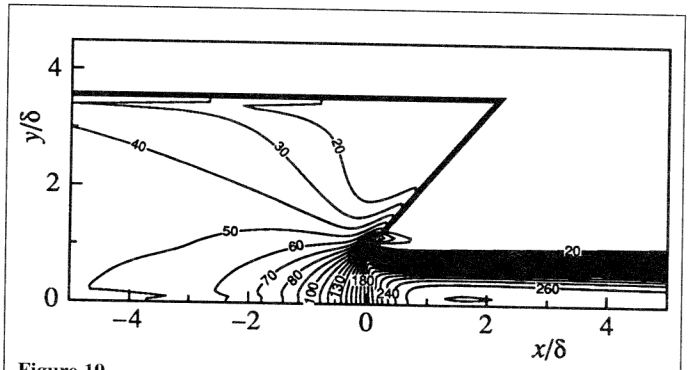

Figure 19.
Flow-velocity contours for a steady two-dimensional subsonic orifice flow with a free jet (half-width $\delta = 2.54$ cm).

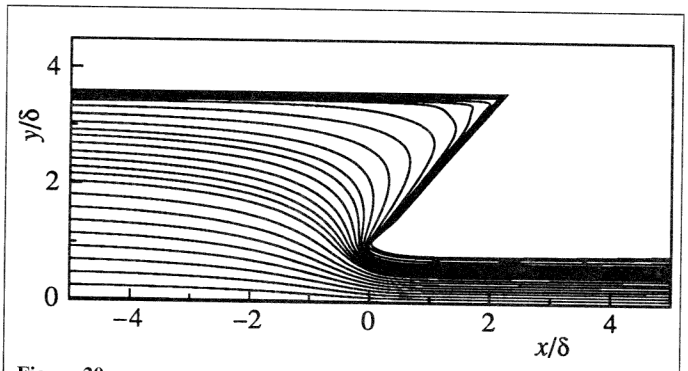

Figure 20.
Flow streamlines for a steady two-dimensional subsonic orifice flow with a free jet (orifice half-width $\delta = 2.54$ cm).

Concluding Remarks

Dirichlet boundary solutions for one-dimensional transient flows of thermally and calorically perfect gases in ducts have been presented in terms of Riemann problems for a number of physically different boundaries and/or numerical grid truncations. These boundary-condition solutions are very useful when solving unsteady one-dimensional flows in shock tubes, hypersonic impulse tunnels, blast simulators, blow-down wind tunnels, solid-propellant rocket motors, and in the pipes of reciprocating pumps and combustion engines. They are ideally suited in applications of explicit numerical techniques that make use of exact Riemann solvers, such as the random-choice method and Godunov finite-difference scheme, but they may also be employed with other finite-volume, finite-difference, and finite-element based solution procedures. Furthermore, although the boundary conditions have been derived with the specific intention of treating flows having variations in only one spatial dimension, their usefulness in multi-dimensional flow prediction, for cases where locally one-dimensional flow approximations are appropriate, has also been demonstrated.

The present boundary solutions for the duct end open to an atmosphere or a finite-volume reservoir have been derived by using the quasi-steady assumption that the flow at the boundary responds instantly to the surrounding atmospheric conditions, whereas in practice there is a response delay. Rudinger (1957, 1958, 1961a, 1961b) has shown that the time delay depends not only on the flow conditions at the boundary but also on its previous flow history. His analysis by the method of characteristics for this delayed response has not been included in the open end boundary conditions described herein, primarily because an implementation has not yet been made practical for general numerical methods. The effects of neglecting the time delay are important only in predicting accurate unsteady flow solutions very near the open duct end, when the moving shock or rarefaction wave is strong, or it has a short wavelength (i.e., the pressure changes rapidly across the wave front as it passes through the open end).

Acknowledgements

Funding for this research from the Natural Sciences and Engineering Council of Canada by means of Operating Grant No. OGP–0004539 is gratefully acknowledged. The interest in this work and encouragement by David R. Greatrix and Chak Man Tsui are much appreciated.

REFERENCES

[1]Ali, M.A., Gill, K.F., and Imrie, B.W., "The Effect of Mass Flow Rate on the Reflection Behaviour of Small-Amplitude Pressure Waves from Duct Terminations," *Journal of Mechanical Engineering Science*, Vol. 20, pp. 229-235, 1978.

[2]Bannister, F.K., and Mucklow, G.F., "Wave Action Following Sudden Release of Compressed Gas from a Cylinder," *Proc. Instn. Mech. Engrs.*, Vol. 159, pp. 269-300, 1948.

[3]Benson, R.S., "Experiments on Two-Stroke Engine Exhaust Ports Under Steady and Unsteady Flow Conditions," *Proc. Instn. Mech. Engrs.*, Vol. 173, pp. 511-536, 1959.

[4]Chorin, A.J., "Random Choice Solution of Hyperbolic Systems," *Journal of Computat. Phys.*, Vol. 22, pp. 517-533, 1976.

[5]Clarke, J.F., "Regular Reflection of a Weak Shock Wave from a Rigid Porous Wall," *Quarterly Journal of Applied Mathematics*, Vol. 37, pp. 87-110, 1984.

[6]Clarke, J.F., "The Reflection of Weak Shock Waves from Absorbent Surfaces," *Proc. Royal Soc. London* A, Vol. 396, pp. 365-382, 1984.

[7]Clarke, J.F., "Reflection of a Weak Shock Waves from a Perforated Plug," *Journal of Engin. Math.*, Vol. 18, pp. 335-349, 1984.

[8]Colella, P., "Glimm's Method for Gas Dynamics," *SIAM Journal of Scientific and Statistical Computing*, Vol. 3, No. 1, pp. 76-110, March 1982.

[9]Engquist, B., and Majda, A., "Absorbing Boundary Conditions for the Numerical Solutions of Waves," *Math. Comp.*, Vol. 31, pp. 629-651, 1977.

[10]Giles, M.B., "Non-reflecting Boundary Conditions for Euler Equation Calculations," *AIAA Journal*, Vol. 28, pp. 2050-2058, 1990.

[11]Glimm, J., "Solutions in the Large for Nonlinear Hyperbolic Systems of Equations," *Commun. Pure Appl. Math.*, Vol. 18, pp. 695-715, 1965.

[12]Godunov, S.K., "Finite-Difference Method for Numerical Computations of Discontinuous Solutions of the Equations of Fluid Dynamics," *Mat. Sb.*, Vol. 47, pp. 271-306, 1959.

[13]Gottlieb, J.J., "Staggered and Nonstaggered Grids with Variable Node Spacing and Local Time Stepping for the Random Choice Method," *Journal of Computat. Phys.*, Vol. 78, pp. 160-177, 1988.

[14]Gottlieb, J.J., and Groth, C.P.T., "Assessment of Riemann Solvers for Unsteady One-Dimensional Inviscid Flows of Perfect Gases," *Journal of Computat. Phys.*, Vol. 78, pp. 437-458, 1988.

[15]Groth, C.P.T., "TVD Flux-Difference Split Methods for High-Speed Thermochemical Nonequilibrium Flows with Strong Shocks," Report 350, University of Toronto Institute for Aerospace Studies, Dec. 1993.

[16]Groth, C.P.T., and Gottlieb, J.J. , "Numerical Study of Two-Stage Light-Gas Hypervelocity Projectile Launchers," Report 327, University of Toronto Institute for Aerospace Studies, Oct. 1988.

[17]Gustafsson, B., Kreiss, H.-O., and Sundström, A., "Stability Theory of Difference Approximations for Mixed Initial Boundary Value Problems II," *Math. Comp.*, Vol. 26, pp. 649-686, 1972.

[18]Hedstrom, G.W., "Nonreflecting Boundary Conditions for Nonlinear Hyperbolic Systems," *Journal of Computat. Phys.*, Vol. 30, pp. 222-237, 1979.

[19]Higdon, R.L., "Initial-Boundary Value Problems for Linear Hyperbolic Systems," *SIAM Rev.*, Vol. 28, pp. 177-217, 1986.

[20]Kamowitz, D., "Some Observations of Boundary Conditions for Numerical Conservation Laws," Report 88-67, ICASE, Nov. 1988.

[21]Karni, S., "To the Boundary and Back—A Numerical Study," *Int. Journal of Numer. Meth. Fluids*, Vol. 13, pp. 201-216, 1991.

[22]Kreiss, H.-O., "Initial Boundary Value Problems for Hyperbolic Systems," *Commun. Pure Appl. Math.*, Vol. 23, pp. 277-298, 1970.

[23]Mucklow, G.F., and Wilson, A.J., "Wave-Action in Gases: The Attenuation and Reflection of Compression Waves Propagating in Pipes," *Proc. Instn. Mech. Engrs.*, Vol. 169, pp. 69-82, 1955.

[24]Porter, R.W., and Coakley, J.F., "Use of Characterisitics for Boundaries in Time Dependent Finite Difference Analysis of Multidimensional Gas Dynamics," *Int. Journal of Numer. Meth. Engin.*, Vol. 5, pp. 91-101, 1972.

[25]Roe, P.L., "Approximate Riemann Solvers, Parameter Vectors, and Difference Schemes," *Journal of Computat. Phys.*, Vol. 43, pp. 357-372, 1981.

[26]Roe, P.L., and Pike, J., "Efficient Construction and Utilisation of Approximate Riemann Solutions," In R. Glowinski and J.L. Lions, Eds., *Computing Methods in Applied Science and Engineering*, Vol. VI, pp. 499-518, Amsterdam, North-Holland, 1984.

[27]Rudinger, G., "Nonsteady Flows in Ducts, Wave-Diagram Analysis," *Dover Publications,* New York, 1955.

[28]Rudinger, G., "On the Reflection of Shock Waves from an Open End of a Duct," *Journal of Appl. Phys.*, Vol. 26, pp. 981-993, 1955.

[29]Rudinger, G., "A Flow Instability Following Shock Reflection from a Flared End of a Duct," *Jet Propulsion*, Vol. 25, pp. 541-543, 1955.

[30]Rudinger, G., "Improved Wave Diagram Procedure for Shock Reflection from an Open End of a Duct," *Journal of Appl. Phys.*, Vol. 26, pp. 1339-1341, 1955.

[31]Rudinger, G., "The Reflection of Pressure Waves of Finite Amplitude from an Open End of a Duct," *Journal of Fluid Mech.*, Vol. 3, pp. 48-66, 1957.

[32]Rudinger, G., "The Reflection of Shock Waves from an Orifice at the End of a Duct," *ZAMP*, Vol. 1Xb, pp. 570-585, 1958.

[33]Rudinger, G., "Nonsteady Supercritical Discharge Through an Orifice," ASME Transactions, *Journal of Basic Engineering*, Paper No. 61-HYD-17, pp. 1-8, 1961.

[34]Rudinger, G., "Nonsteady Discharge of Subcritical Flow," ASME Transactions, *Journal of Basic Engineering*, Paper No.60-WA-152, pp. 341-348, 1961.

[35]Rudinger, G., "Effect of Boundary Layer Growth in a Shock Tube on Shock Reflection from a Closed End," *Phys. Fluids*, Vol. 4, pp. 1463-1473, 1961.

[36]Sod, G.A., "A Numerical Study of a Converging Cylindrical Wave," *Journal of Fluid Mech.*, Vol. 83, pp. 785-794, 1977.

[37]Sweby, P.K., "High Resolution Schemes Using Flux Limiters for Hyperbolic Conservation Laws," *SIAM Journal of Numer. Anal.*, Vol. 21, pp. 995-1011, 1984.

[38]Thompson, K.W., "Time Dependent Boundary Conditions for Hyperbolic Systems," *Journal of Computat. Phys.*, Vol. 68, pp. 1-24, 1987.

[39]Zhang, K.Y., and Gottlieb, J. J., "Simulation of a Blast Wave in a Shock Tube by Using Perforated Plates in the Driver," Report 304, University of Toronto Institute for Aerospace Studies, March 1986.

[40]Zucrow, M.J., and Hoffman, J.D., "Gas Dynamics," Vols. 1 and 2, John Wiley and Sons, New York, 1976 and 1977.